Study of the effects of trapped compression ratio on the heavy fuel operation of a spark ignition Unmanned Aerial Vehicle engine

Journal:	*Aircraft Engineering and Aerospace Technology*
Manuscript ID	AEAT-07-2021-0220.R2
Manuscript Type:	Research Paper
Keywords:	Heavy fuel engine, JET A-1, kerosene spark ignition, UAV engine, Unmanned Aerial Vehicle, two-stroke cycle engine

Study of the effects of trapped compression ratio on the heavy fuel operation of a spark ignition Unmanned Aerial Vehicle engine

Abstract

Purpose – This paper aims to present experimental experience of heavy fuelling of a spark ignition crankcase scavenged two-stroke cycle Unmanned Aerial Vehicle engine, particularly focusing on the effects of compression ratio variation and to cross correlate with the results of fluid dynamic modelling of the engine and fuels used.

Design/methodology/approach – One-dimensional modelling of the engine has been conducted using WAVE software supported by experimental dynamometer testing of a spark ignition UAV engine to construct a validated computational model using gasoline and kerosene JET A-1 fuels.

Findings – The investigation into the effects of compression ratio variation via fluid dynamic simulation and experimental testing has allowed an assessment of the approach for improving heavy fuel operation of UAV engines using auxiliary transfer port fuel injection. The power level achieved with reduced compression ratio heavy fuel operation is equal to 15.35 kW at 6500 RPM compared to 16.27 kW from the standard gasoline engine or a reduction of 5.7%.

Practical implications – The studied engine is specifically designed for UAV applications. The validation of the computational models to explore the effects of compression ratio and heavy fuel injection on the solution and cost is supported by experimental tests.

Originality/value – The application of auxiliary port fuel injection of heavy fuel and associated compression ratio optimisation offers an alternative approach to achieve the safety and logistical challenges of the single fuel policy for UAVs. The application of WAVE to simulate crankcase scavenged two-stroke cycle engines has been applied in very few cases. This study shows further exploratory work in that context.

Keywords *Heavy fuel engine, JET A-1, kerosene spark ignition, engine modelling, internal combustion engine, two-stroke cycle engine, UAV engine, UAS engine.*

Paper type Research paper

Introduction

The single fuel policy (US DoD (1988)) as discussed by Owens *et al* (1989) has to some extent been successfully implemented for some elements of military equipment, however; key areas still remain a challenge as discussed by Duddy *et al* (2011) and Hooper (2017a). Unmanned Aerial Systems (UAS) or unmanned aerial vehicles (UAV) are such an area. The majority of systems operating at medium to low altitude are predominantly systems operating with gasoline fuelled internal combustion engines as demonstrated by the AAI Shadow RQ-7, Elbit Hermes 450/Thales Watchkeeper, IAI Heron and General Atomics MQ-1 air vehicles (Austin, 2010). Gasoline is a readily available fuel providing good performance levels, however; in a military theatre of operations its use presents major logistical and safe operational problems as discussed by Davis (1991) and Malriat *et al* (1991). Several engine research programmes have explored adaptation of pre-existing UAV engines using four-stroke cycle and two-stroke cycle power plants as indicated by the research of Xu *et al* (2021) and the Ricardo Wolverine 3 engine as discussed by Liu *et al* (2019). These programmes have included conventional reciprocating piston technology as demonstrated by the work of Blank *et al* (2001) and Duddy *et al* (2011). Wankel rotary engines, which operate on a four-stroke cycle, have also been considered as reported by Kweon (2011) and Kucinski (2018). Four-stroke compression ignition diesel engines have seen some successful introduction into larger aircraft as indicated by the research of Goraj and Frydrychewicz (2004). Four-stroke engines, with the same number of cylinders, exhibit significantly inferior vibration characteristics than two-stroke engines as discussed by Hooper (2019). Some studies have considered unconventional technologies to successfully address the challenge as demonstrated by the research of Kalkstein (2006) using opposed piston engine technology and that of Hooper *et al* (2012) building upon the prior research work of Hooper and Favill (1978) with segregated scavenging for higher durability.

Turbine engines have also been considered for smaller UAVs as demonstrated by the work of Turan (2012) and McDonald *et al* (2008) with some success. Turbines are perhaps better suited to operate on low volatility fuels and are designed to function most efficiently on such fuels, however; for UAV application their loiter speeds can be a limiting factor unless a rotary wing solution is adopted. Piston engine UAVs are more readily suited for slower loitering speeds over a designated target position. The high specific fuel consumption of small turbines is also a limiting factor in their application to small air vehicles.

The low volatility fuels considered for UAVs include kerosene-based fuels such as JP-5, JP-8, AVTUR and JET A-1 and diesel fuels such as DF2. The fuel forming the feed stock in this study is kerosene JET A-1. All of these fuels present advantages over gasoline in terms of safer storage and supply, a key benefit when having to move fuel to forward operating positions. A further advantage is in terms of logistics. The only military systems requiring gasoline was motorcycles, light all-terrain vehicles, outboard motors and UAVs. Research and development has successfully resolved or provided potential solutions to all but the UAV application as presented by Work (2011). For this reason, gasoline is naturally seen as a seriously problematic fuel requiring special treatment especially onboard Navy vessels with contingency plans in place to jettison the stock in cases of emergency.

By the very nature of the fuels considered so far, their low volatility presents serious challenges in terms of achieving cold starting, acceptable levels of operational performance and avoiding the onset of combustion knock or detonation in spark ignition engines. Cold starting has been demonstrated to be achievable via the research of Hooper (2017a), Hooper and Al-Shemmeri (2017b) and Liu *et al* (2016). Achieving good performance levels whilst avoiding detonation is essential. Combustion knock will destroy an internal combustion engine. Continued operation in conditions provoking the onset of knock can result in an avalanche effect resulting in localised overheating of critical exposed areas of pistons, combustion chamber surfaces and premature bearing failure due to the higher loading experienced by the small end bearing in particular.

Significant difficulties in terms of detonation naturally exist for Wankel type rotary combustion engines due to the shape of the combustion chamber. The inherently long flame path, usually inevitable with rotary combustion engine arrangements, leads to heightened susceptibility to the engine type suffering from combustion knock occurrence. This is a consequence of the unavoidably long distances to the cool end gas location with the rectangular profile of the chamber section. Detonation can also be a major problem for conventional piston engines but it is often easier to design the engine to secure a relatively short flame path to the extremities of the chamber.

The most effective fuelling system in terms of maximising thermal efficiency for a two-stroke cycle engine has largely been demonstrated by adoption of direct injection as shown by the research of Duret (1988), Schlunke (2001) and more recently by Turner *et al* (2010), Blundell *et al* (2010) and discussed by Hooper *et al* (2011, 2012) and Stone (2012). More recently Matarelli *et al* (2014) have discussed concepts of applying DI to two-stroke engines for automotive application. Unfortunately, direct injection hardware suffers a greater mass penalty when compared with low pressure fuel injection systems delivering fuel via the inlet port or further upstream via the transfer ports. This penalty is due to the nature of the combustion pressure/heat exposure of the injectors and that higher fuel delivery pressures are normally required for DI. This is of course offset to an extent by the lower fuel payload secured by the increased thermal efficiency but nevertheless a trade off becomes apparent for the UAV system integration adopted.

This paper focuses on application of low-pressure fuel injection of kerosene JET A-1 into the transfer port area of a two-stroke cycle UAV engine to assess the feasibility of operation of the engine on heavy fuel. Experimental testing of the engine and further supporting modelling of the engine using proprietary well respected engine simulation software in order to simulate engine modifications and explore correlation between the real and virtual engines.

Methodology

A twin cylinder 342 cm^3 crankcase scavenged two-stroke engine was used for this study. The basic form of the engine uses a single diaphragm carburettor supplying a common crankcase. The engine was therefore modified to allow installation of low-pressure auxiliary port injection (API). A cross-sectional arrangement of the engine arrangement is shown for reference in Figure 1.

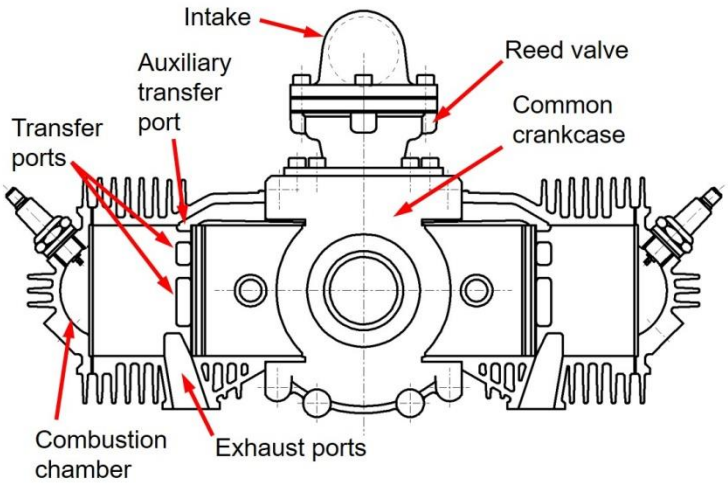

Figure 1. Engine sectional arrangement

As can be seen in Figure 1, the engine is a 180° horizontal flat-twin design and employs a shared crankcase providing scavenge air for both cylinders. Each cylinder of the engine displaces a swept volume of 171 cm^3.

The dynamometer installation of the engine can be seen in Figure 2.

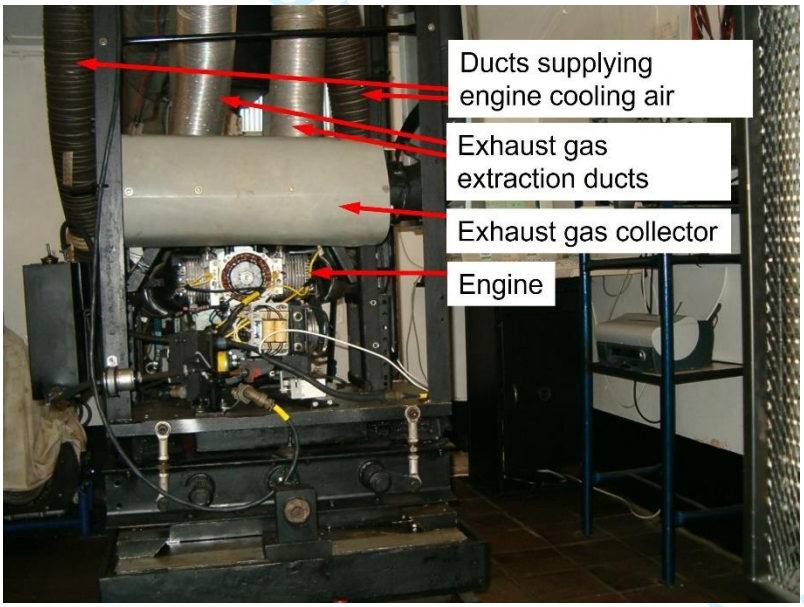

Figure 2. Engine dynamometer installation

Cooling air was ducted to the engine via flexible ducts to each individual cylinder. The air being supplied via a variable speed centrifugal blower with air ducted to the blower intake from outside the test cell. The standard engine was originally designed to operate with short stub exhaust pipes. In order to accommodate the same system for experimental testing an exhaust gas collector/muffler was fabricated and positioned close to the engine in order to collect and safely extract exhaust gases out of the test cell. A schematic of the test cell arrangement providing more details of the experimental test installation is shown in Figure 3.

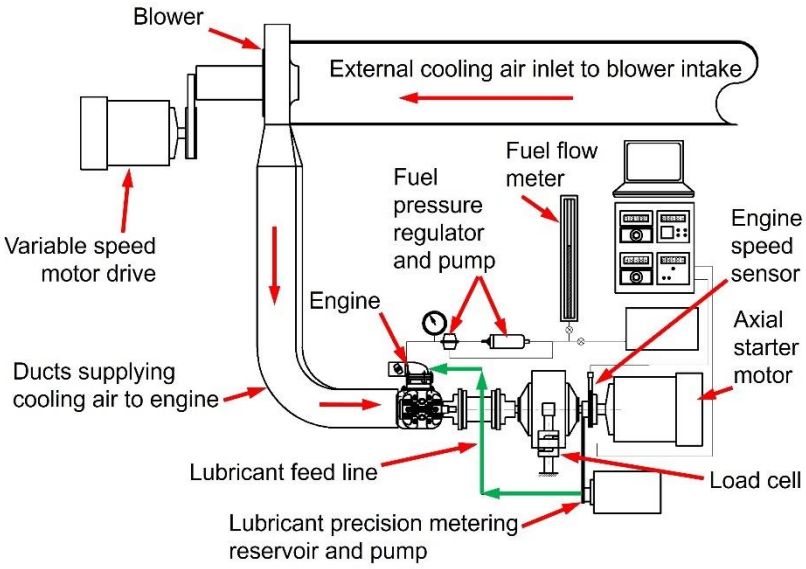

Figure 3. Engine dynamometer arrangement (Exhaust extraction system removed)

For clarity Figure 3 does not show the exhaust gas collector/muffler and extraction system. In terms of fuel supply, any excess fuel not consumed by the engine is recirculated to fuel pump intake thereby allowing the fuel meter to assess the flow rate of fuel actually entering the engine directly.

Design characteristics for the standard engine are provided in Table 1.

Table.1. Standard engine design data

Swept Volume (cm^3)	342
No. of cylinders	2
Bore (mm)	66
Stroke (mm)	50
Trapped compression ratio (r_{cTrap})	7.1:1
Crankcase compression ratio (r_{cc})	1.5:1
Induction control	Single 6 petal reed valve (steel reeds)
Fuel system	Single diaphragm carburettor
Alternative fuel system	Single point inlet injection upstream of the crankcase
Fuel	Gasoline (with 4% SAE40 two-stroke oil added)
Lubrication system	Total loss (Premixed fuel)
Exhaust system	Short stub pipes

One-dimensional Engine Modelling

The fluid dynamics models of the engine were developed using WAVE (version 2021.3), the one-dimensional code developed by Ricardo (2022). The layout of the representative model can be seen in Figure 4.

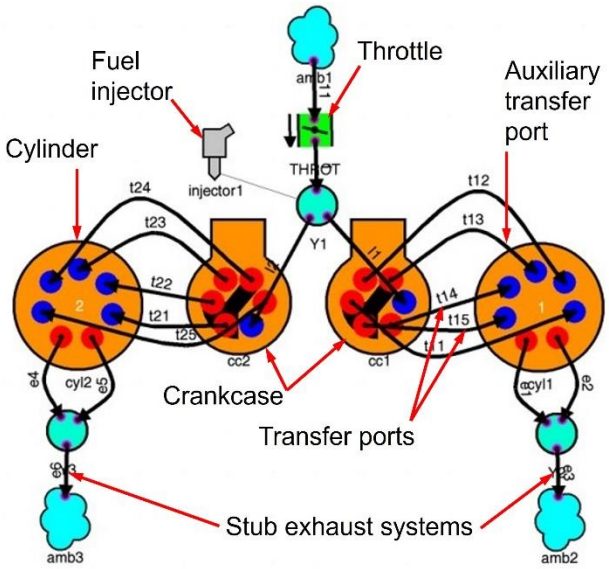

Figure 4. Engine one-dimensional model

The common intake manifold and reed valve block was reflected within the models; however, it was not possible to model the two cylinders from a single crankcase. A model using two crankcases was developed as shown in Figure 4 to circumvent this. The two systems were developed to replicate the compression ratio of the single common crankcase of the real engine. The cylinders use a five-transfer port arrangement that adopts the loop scavenging process developed originally by Schnürle as discussed by Schweitzer (1949) and Hooper (2017a). Each of the ports can be seen to be connected to the crankcases by passages or ducts. Auxiliary transfer port fuel injected models replicated the positioning of the injector at a position 5mm from the cylinder end of the port and therefore close to piston. The injector pulse width was optimised within the model. For inlet injected models a single injector was located feeding into the Y junction between the throttle and crankcase as shown in Figure 4. In response to the computed air mass flow, fuel flow was calculated proportional to a pre-set stoichiometric air:fuel ratio defined within the model. The engine also uses two exhaust ports per cylinder with a central bridge exhausting into short stub pipes of 122 mm length and this arrangement has been recreated in the models.

Model theory

Many two-stroke cycle engines utilise reed valves in order to control the induction charge flow. The engine forming the subject of this study uses a single block six petal reed valve for such purpose feeding the common crankcase. In other words, this single block controls the entire engine air flow or air and fuel for the carburetted or inlet injected engine. The theory behind modelling the reed valve has been previously discussed by Hooper and Al-Shemmeri (2017) building upon the prior research of Morrison *et al* (1971) and Hinds (1978). The reed can be considered as a cantilever of slender cross section. The steel reeds applied in this study were 17.5 mm wide, 25 mm effective length and 0.2 mm thick. Using cantilever beam theory, it is possible to consider the reed motion due to the pressure difference occurring across the valve. Based upon the reed stiffness, the lift and open area at any condition can be calculated. The expression in equation (1), as defined by Morrison *et al* (1971), can be used to determine deflection at the reed tip: -

$$r_{tip} = \frac{\Delta p_r w_r l_r}{8EI} \tag{1}$$

In terms of flow through the reeds, Morrison *et al* (1971) showed that the flow time area can then be calculated from equation (2): -

$$\int A d\theta = \frac{n_r r_{tip} P_w \theta_p}{2} \tag{2}$$

Based upon the work of Hinds (1978), the reed natural frequency can be calculated from equation (3). Values for the $\beta_j l_r$ term in equation (3) relate to the reed modes of vibration with values of 1.875, 4.694, 7.855, 10.996 and 14.137 recommended. Higher than fifth order values can be ignored as discussed by Blair (1996) and Hinds (1978).

$$f_r = \frac{(\beta_j l_r)^2}{2\pi}\sqrt{\frac{EI}{p_r A_b l_r^4}} = \frac{(\beta_j l_r)^2}{2\pi}\sqrt{\frac{Et_r^2}{12 p_r l_r^4}} \tag{3}$$

The reed spring constant, k_r, can be determined from computing equations (3) and (4): -

$$f_r = \sqrt{\frac{k_r}{m_r}} \tag{4}$$

Input of the effective port flow area and reed spring constant, k_r, enables WAVE to simulate the reed block.

The crankcase was modelled as a pump. As previously discussed, two crankcase elements can be seen in Figure 4 whilst only one is employed in the actual engine. Input functions revolve largely around the compression ratio of the crankcase. It was deemed acceptable to continue the model build with two crankcases with the same crankcase compression ratio as that measured from the original engine. The crankcase provides pressurised air to the five transfer ports located in the cylinders. Combustion is spark initiated with spent gas exhausted from the cylinders via two exhaust ports. The flow time-area history of transfer and exhaust ports can be seen in Figure 5.

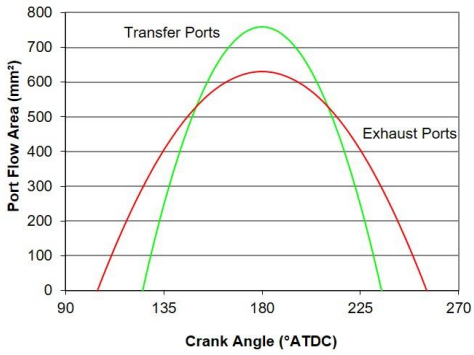

Figure 5. Port flow time - area history

Within a two-stroke cycle engine equipped with ports in the cylinder walls, the flow of air/exhaust is defined by the gas properties and the position of the piston. Port effective flow area can be defined by determining their discharge coefficients (*Cd*) at varying port opening or piston positions. However, Blair (1996) argues that whilst this approach can be used effectively to improve port flow characteristics, it is of limited assistance within one-dimensional fluid dynamic engine models due to limitations of the models to be able to reproduce the actual thermodynamics occurring within the real engine. For this reason, isentropic methods can be adopted.

The port flow area and associated mass flow can be calculated from equations (5) and (6) respectively, as developed by Heywood and Sher (1999): -

$$A_o = w_p h_o - r_p^2\frac{[4-\pi]}{2} \tag{5}$$

$$\dot{m} = \frac{C_d A_r p_o}{\sqrt{RT_o}}\left(\frac{p_R}{p_o}\right)^{\frac{1}{\gamma}}\sqrt{\frac{2\gamma}{\gamma-1}\left(1-\left(\frac{p_R}{p_o}\right)^{\frac{\gamma-1}{\gamma}}\right)} \tag{6}$$

Heywood and Sher (1999) also discuss that for sonic flow, the mass flow is defined by equation (7): -

$$\dot{m} = \frac{C_d A_r p_o}{\sqrt{RT_o}} \sqrt{\gamma} \left(\frac{2}{\gamma + 1} \right)^{\frac{\gamma+1}{2(\gamma-1)}} \tag{7}$$

When computing cylinder flow via transfer ports, the pressure p_R is taken to be the value occurring in the cylinder whilst stagnation pressure, p_o, is set to the scavenge flow pressure. For exhaust flow via the exhaust ports, the stagnation pressure, p_o, is conversely set at the cylinder pressure and p_R, is set to the exhaust pressure. As the port pressure ratio varies the C_d value varies significantly. Heywood and Sher (1999) found that the steady flow C_d value is normally higher than the comparative value determined via unsteady flow conditions. Within WAVE it is possible to define flow coefficients where data is available. A key input function was taken from the engine porting analysis shown in Figure 5 to define flow areas and timing of all modelled ports.

The work of Wiebe (1967) established the formula in equation (8) for assessment of the mass fraction burnt by the combustion process. This formula forms the basis of calculations within WAVE. Ghojel (2010) further discusses the research of Wiebe.

$$x(\theta) = 1 - exp\left[-\left[\frac{c(\theta - \theta_0)}{\Delta\theta_b} \right]^{-b} \right] \tag{8}$$

The research of Heywood and Sher (1999) analysing similar crankcase scavenged spark ignition two-stroke cycle engines has been used to influence the Wiebe function development within this study. Sher (1984) identified values for *b* and *c* of 5 and 3 to 3.2 respectively following combustion rate analysis of the engines in question. In the absence of specific data for the subject engine this prior research has been considered here.

A critical aspect of any engine model is within the assumptions for heat transfer. In the WAVE models the following calculation for heat transfer coefficient, *h*, was used: -

$$h = 0.0128\ D^{-0.2}\ P^{0.8}\ T^{-0.53}\ v_{ch}{}^{0.8} C_m \tag{9}$$

Equation (9) is derived from the research of Woschni (1967). The mean piston speed was found by Woschni to be able to equate to the characteristic gas speed, v_{ch}. The variable C_m, in equation (9) is a scaling factor based upon cylinder bore diameter. If for example the piston crown has a flat non-domed design the value for C_m would be unity, as it was for the subject engine. The combustion chamber is a concentric recess as can be seen in Figure 1. The surface area of the chamber was analysed resulting in a value for C_m of 1.315.

The Colburn analogy as defined by Bird *et al* (2002), and shown in equation (10), is used by WAVE to calculate heat transfer in areas remote from the cylinder.

$$h = \frac{C_f}{2} p U c_p P_r^{-\frac{2}{3}} \tag{10}$$

An allowance for engine friction within WAVE is provided by the expression developed by Chen and Flynn (1965) and shown in equation (11). Unfortunately, Morse test (Stone, 2012) data was unavailable for the engine so values for friction mean effective pressure (p_f) typical for crankcase scavenged engines were used in this study to make the correlation representative here.

$$p_f = c_1 + c_2(p_{max}) + c_3 \frac{Ns}{2} + c_4 \left(\frac{Ns}{2} \right)^2 \tag{11}$$

The WAVE combustion knock sub-model used for the research presented in this Paper is based upon the induction time correlation developed by Douaud and Eyzat (1978). At each timestep within the model the ignition delay or induction time, τ, is calculated via the expression shown in equation (12): -

$$\tau = 0.01869 A_p \left(\frac{O_N}{100}\right)^{3.4017} p_{cyl}{}^{-1.7} \, exp\left(\frac{3800/A_T}{T_{unb}}\right) \quad (12)$$

A key input to equation (12) is the octane number, O_N, of the fuel defined by the user in the WAVE model. A_p is a multiplier defined by the user, p_{cyl} is the cylinder pressure, A_T is a user entered multiplier for activation temperature and T_{unb} is the temperature of the unburned gas fraction in the cylinder. When knock is detected, the user is notified.

As the combustion cycle advances the ignition delay, τ, reduces and the temperature increases in the unburnt mixture. If the flame arrival time is greater than the induction time auto-ignition will occur or when the condition defined by equation (13) is met: -

$$\int_{t_0}^{t_i} \frac{d\tau}{\tau} = 1 \quad (13)$$

The integral limits defined by equation (13) are the auto-ignition (t_i) and end gas compression (t_o) start points. During the simulation the integral is evaluated with time, t_i, being the current instantaneous time of the simulation. Time, t_i, is then ultimately determined when the integral reaches the unity value.

A post detonation burn acceleration can be defined. When this is set, a rate of burn for the spontaneous combustion mass is returned to the cylinder. This causes an increase in temperature and pressure in the cylinder and an increase in heat transfer coefficient within the cylinder. This then defines a post detonation burn time, τ_{post}, defined by equation (14): -

$$\tau_{post} = f_t \left[\frac{0.8573}{B_0(1+A/F)} exp\left(\frac{T_{act}}{T_{af}}\right)\right] \quad (14)$$

In equation (14); f_t, is a multiplier for the burn scale for post knock occurrence, B_0, is a frequency factor (2233 x 10^3 Hz), A/F, is the air:fuel ratio, T_{act}, is the activation temperature and T_{af}, is the adiabatic flame temperature.

During the post knock phase the rate of fuel burn is calculated from equation (15): -

$$\dot{m}_{fuel} = \frac{m_{vap}+m_{liq}}{\tau_{post}} \quad (15)$$

Similarly the burn rate of the air in the cylinder is calculated from equation (16): -

$$\dot{m}_{air} = \dot{m}_{fuel}(A/F) \quad (16)$$

In equation (15) m_{vap} and m_{liq} are the unburned fuel vapour and unburned liquid fuel masses at the point of knock occurrence. The formulae presented in equations (11) to (16) were developed by Douaud and Eyzat (1978).

The modelling and experimental work presented in this paper builds upon the prior published work of Hooper and Al-Shemmeri (2017c).

Results

Gasoline baseline testing with the standard Mikuni BN-34-30 carburettor was established to 7000 RPM with and without a low resistance exhaust system collector/muffler, fabricated in order to reduce noise levels. This was done to ensure that the collector/muffler system was not affecting the engine's normal operation with the standard 122 mm stub pipes. The results of initial baseline tests are shown in Figure 6. The experimental test

data was recorded using 98RON gasoline with synthetic two-stroke oil added to the fuel in the recommended ratio of 25:1.

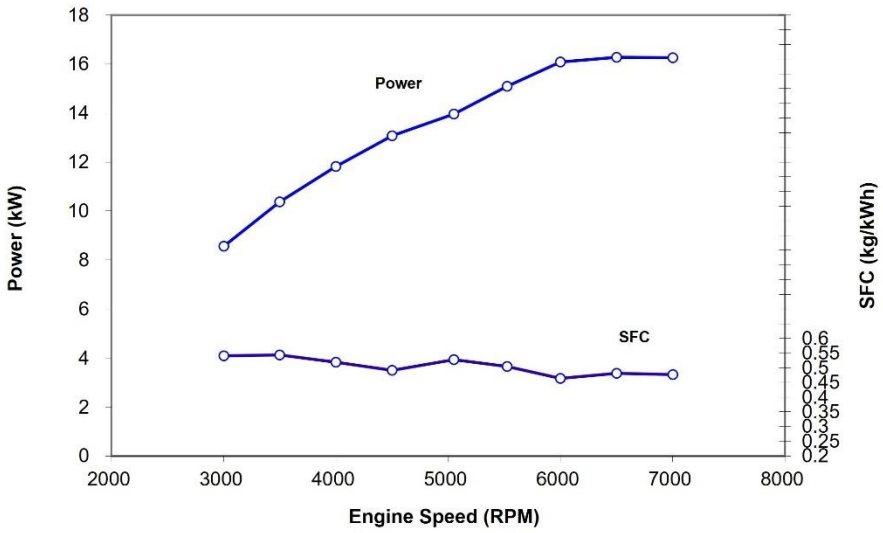

Figure 6. Initial experimental baseline test data of engine recorded using carburettor fuelling with 98RON gasoline with 25:1 oil premix

On reference to Figure 6, the maximum power from the experimental testing can be seen to occur at 6500 RPM with a value of 16.27 kW. The minimum full load SFC occurs at 6000 RPM with a value of 0.464 kg/kWh.

Testing with indirect injection into the auxiliary transfer ports was then performed. Again the fuel used was 98RON gasoline but as this point of fuel introduction bypasses some of the critical components that require the oil for lubrication an alternative means of lubrication was required. A precision metering system was calibrated in order to provide a separate supply of lubricating oil into the intake manifold just upstream of the engine reed valve. This was metered to replace the 4% oil that would otherwise be present in the intake fuel supply. The pump was driven from the dynamometer shaft as shown in Figure 3 to simplify the installation. Oil delivery was fed to the common intake manifold just upstream of the reed valve.

Auxiliary port fuel injection (API)

Injection of fuel via the transfer port area of a two-stroke engine involves a limited time availability for successful unhindered delivery of the fuel charge. Injection has to be synchronised with the port open phase defined by the period of the piston uncovering the port on the down stroke and closing the port on the up stroke. The time window is far less constrained with direct injection (DI) into the combustion chamber, however; DI systems can present a higher mass penalty in terms of the associated hardware required.

Initially relatively low flow rate injectors were used as the metering supply. Unfortunately the delivery at normal operating pressures of 2.75 bar were insufficient. Fuel pressure was increased to 7.25 bar to reduce injector pulse widths. Larger capacity injectors were then installed which were capable of supplying sufficient fuel in the short time available. Figure 7 shows kerosene performance data for the engine using the lower capacity L231 injectors at 7.25 bar, and higher capacity R588 injectors at 2.75 bar.

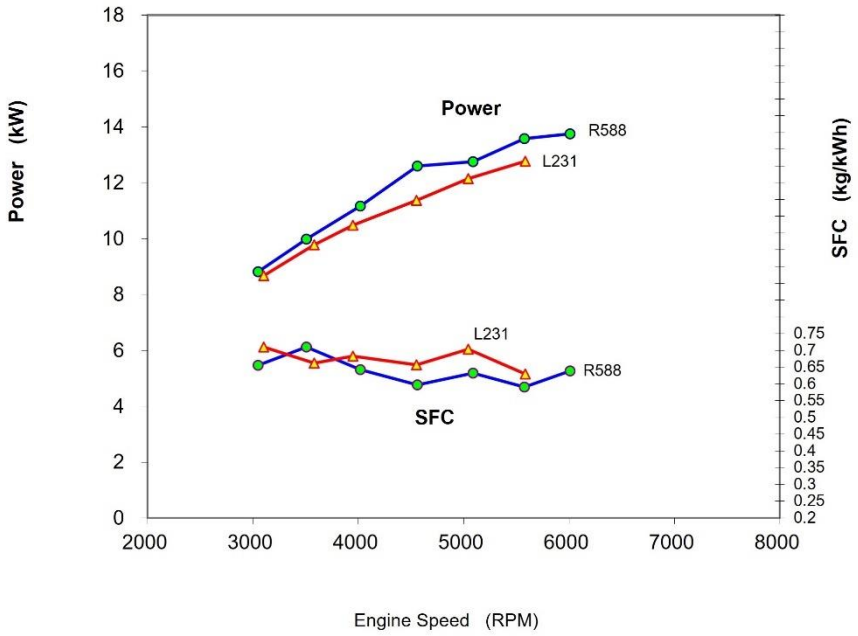

Figure 7. Comparison of experimental kerosene JET A-1 performance using high (R588) and low (L231) flow rate injectors

Initial testing on kerosene was limited to speeds of 6000 RPM due to the onset of combustion knock above 6100 RPM. Using the lower capacity injectors, 5500 RPM was found to be the limiting speed achievable before knock was observed. It should be pointed out that testing below 3000 RPM would usually exhibit increased knock intensity and for this reason the full load engine speed was only explored from 3000 RPM and above. On reference to Figure 7, full load performance at 5000 RPM is 12.14 kW and SFC 0.704 kg/kWh using the L231 injectors, with 12.76 kW and SFC 0.632 kg/kWh using the R588 injectors.

Table 2 shows comparative pulse width and port open time duration for the two injectors.

Table 2. Port Open time and injector pulse width

Engine speed (rpm)	Port Open Time (ms)	L231 injector pulse width (ms)	R588 injector pulse width (ms)
3000	5.50	4.05	3.51
3500	4.71	3.85	3.57
4000	4.13	3.87	3.00
4500	3.67	3.56	2.83
5000	3.30	3.55	2.63
5500	3.00	3.33	2.57
6000	2.75		2.52
6500	2.54		
7000	2.36		

The calculated port open times in Table 2 are determined from the transfer port timing and relevant engine speed. The reduction in port open time with increasing speed can be readily seen. It can also be seen that the injector pulse width with L231 injectors exceeds the port open time above 5000 RPM. Using the R588 injectors with higher flow capacity the reduced corresponding pulse width and hence ability to inject fuel without

impinging on the piston during the port open period is clear to see. This allowed operation up to 6000 RPM and explains the improved SFC observed in Figure 7 with RAM injectors.

One-dimensional modelling of auxiliary port fuel injection

Models of the engine constructed within the architecture of Ricardo WAVE have been configured to examine differing fuel injection methods. A range of models were developed with a pulse width injector located in each auxiliary port.

The model was developed initially to operate on indolene (Zigler *et al* (2011)) fuel, a reference grade form of gasoline. This fuel is a readily available fuel selectable within the WAVE software fuel definition model. It is also possible to generate new fuels, or blends of fuels, using key thermodynamic properties of the fuel. Kerosene JET A-1 was used for all heavy fuel experimental testing and is similar to AVTUR apart from anti-icing inhibitors to allow high altitude military use. After researching relevant data for the properties for the fuel composition (carbon, hydrogen content), lower heating value, density, entropy of formation, specific heat and heat of vaporisation.

Output performance data using inlet injection (II) and auxiliary port fuel injection (API) of indolene is shown in Figure 8. The experimental data recorded with carburetted 98RON gasoline is also shown for comparative purposes.

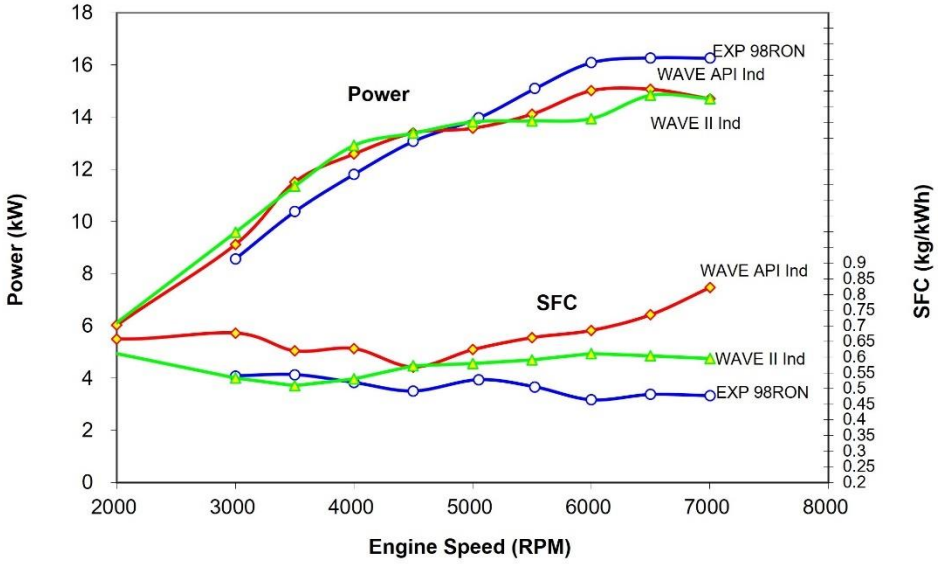

Figure 8. Comparison of 98RON gasoline experimental (EXP) data with WAVE modelled Auxiliary port injection (API) and inlet injection (II) of indolene

It can be seen from Figure 8 that a reasonable correlation between the experimental results and modelled data has been achieved in the medium speed range from 3000 to 5000 RPM although a marked improvement in power with the WAVE model is exhibited at 3500-4000 RPM. Above 5000 RPM the actual data from experimental testing with the diaphragm carburettor demonstrated higher power with a maximum 16.27 kW recorded at 6500 RPM. Using the WAVE models; inlet injected indolene demonstrates a maximum power of 14.84 kW at 6500 RPM whilst auxiliary port injection achieves a higher output of 15.07 kW at 6500 RPM. Specific fuel consumption is lowest with the diaphragm carburettor used in experimental testing with the minimum value being 0.464 kg/kWh occurring at 6000 RPM. A much higher SFC at speeds above 4000 RPM can be seen for inlet injected indolene, although very good correlation can be seen from 3000 – 4000 RPM. On reference to Figure 8 the minimum WAVE modelled SFC with inlet injection can be seen to be 0.508

kg/kWh at 3500 RPM. Using WAVE modelled auxiliary port injection, a significantly higher SFC is evident. The minimum being 0.569 kg/kWh at 4500 RPM.

Predicted cylinder pressure and torque for inlet injection and auxiliary port injection of indolene are presented in Figures 9 and 10 respectively. The data for all cases is at 6000 RPM.

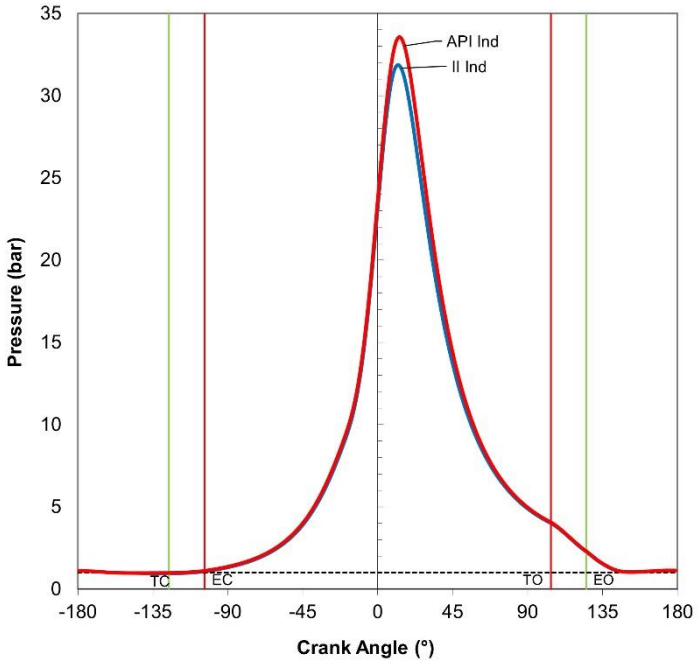

Figure 9. Comparison of cylinder pressures with WAVE modelled Auxiliary port injection (API) and inlet injection (II) of indolene at 6000 RPM

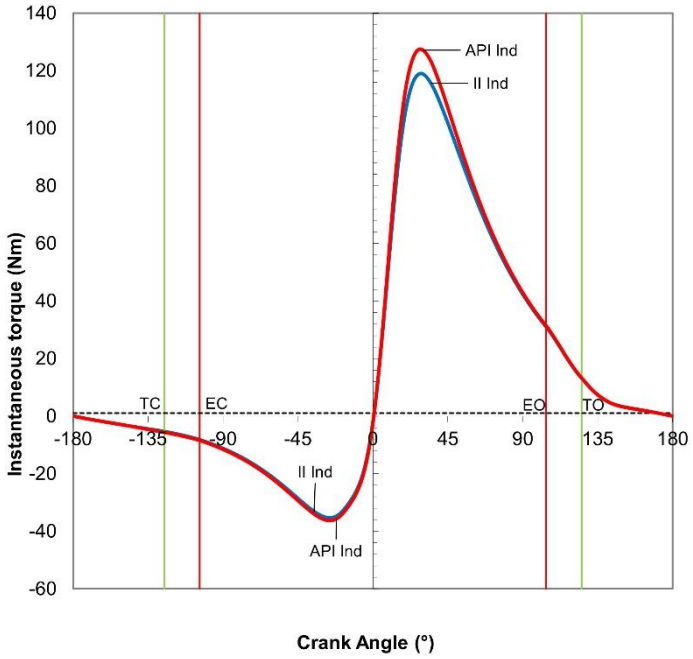

Figure 10. Comparison of instantaneous torque predictions with WAVE modelled Auxiliary port injection (API) and inlet injection (II) of indolene at 6000 RPM

The maximum cylinder pressure, shown in Figure 9, for inlet injection is 31.9 bar occurring at 12.2° ATDC. For the auxiliary port injected model, the maximum cylinder pressure can be seen to have increased to 33.5 bar and occurs at 13.1° ATDC. In terms of the predicted torque throughout the same cycles the peak positive torque is 119.1 Nm for inlet injection with a peak negative of -35.3 Nm. For the higher output observed for API at 6000 RPM the comparable peak values are 127.5 Nm and -36.2 Nm respectively. The positive torque reflects the positive net energy output from the combustion process whilst the negative torque is an indication of the energy input required to perpetuate engine operation during the intake and compression phases of the cycle.

Experimental effects of compression ratio variation

The susceptibility of an internal combustion engine to suffer from combustion knock increases with lower volatility fuels. This has to be eliminated by retarding the ignition timing and/or reducing the compression ratio. For two-cycle engines the most relevant compression ratio is not the full piston stroke ratio, but the trapped compression ratio (r_{cTrap}). The ratio can be calculated from the following expression.

$$r_{cTrap} = \frac{V_{aEC}}{V_c} \tag{17}$$

The engine has a full geometric stroke compression ratio (r_c) of 9.2:1. This equates to a TCR of 6.74:1. From experimental test experience this level was found to be too high for spark ignited kerosene operation. Fortunately, the engine has a detachable cylinder head. This provides simple adjustment of the combustion chamber volume by alteration of the cylinder head gasket/shimming thickness. Alternative shims were machined giving ratios of 6.00:1 (8.02:1) and 5.65:1 (7.28:1). Problems were experienced with the engine head gaskets, so these were later eliminated by use of one-piece copper shim plates.

Table 3. Experimental full geometric and trapped compression ratios

Full geometric compression ratio (r_c)	Trapped compression ratio (r_{cTrap})
9.20:1	6.74:1
8.02:1	6.00:1
7.28:1	5.65:1

Test data is presented in Figure 11, showing the effect of compression ratio adjustment. At 6.00:1 TCR the ignition timing had to be retarded to approximately 50-60% of normal gasoline advance. However further reduction to 5.65:1 enabled advance to normal gasoline ignition timings. At 5000 RPM, the full load performance shown in Figure 11 is 13.56 kW and 0.651 kg/kWh with 6.00:1 TCR and 13.93 kW and 0.610 kg/kWh with 5.65:1 TCR.

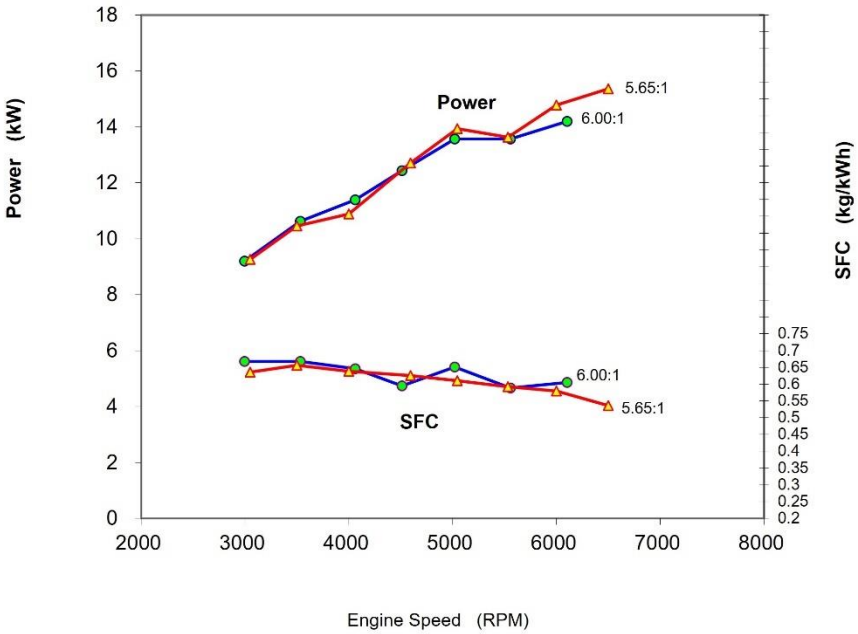

Figure 11. Dynamometer experimental comparison of kerosene JET A-1 injection using 6.00:1 and 5.65:1 trapped compression ratios

One-dimensional modelling of effects of compression ratio variation

Auxiliary port injection of JET A-1

Summarised results of computational modelling of auxiliary port injection (API) of indolene at full compression and JET A-1 at reduced trapped compression ratios of 6.00 and 5.65:1 is compared in Figure 12. Experimental data using carburettor supplied 98RON gasoline is also shown for comparative purposes.

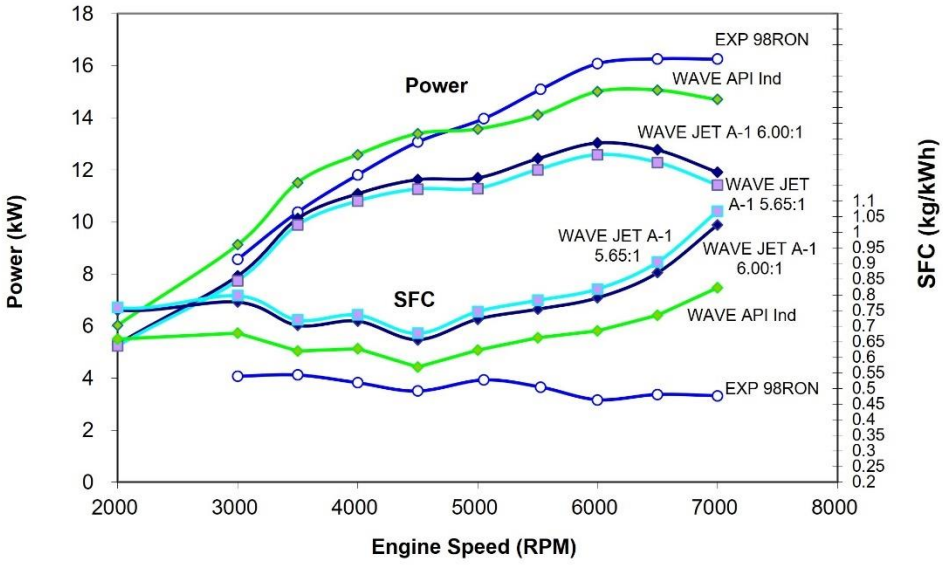

Figure 12. Effect of compression ratio using full compression 98RON gasoline experimental (EXP) data and WAVE modelled Auxiliary port fuel injection of JET A-1 with reduced 6.00:1 (8.02:1) and 5.65:1 (7.28:1) TCR

Simulation data shown in Figure 12 displays the highest maximum power using JET A-1 at 6.00:1 TCR of 13.04 kW at 6000 RPM compared with 12.58 kW at 5.65:1 TCR. The minimum JET A-1 SFC of 0.656 kg/kWh at 4500 RPM is achieved with 6.00:1 TCR compared with 0.677 kg/kWh using 5.65:1 TCR.

WAVE utilises the method of knock prediction derived by Douaud and Eyzat (1978). To determine if knock is occurring WAVE requires values for research octane number (RON) to be input into the activated Douaud and Eyzat sub model. As JET A-1 is not normally used in spark ignition engines no readily available RON values could be located. Contact with Shell Aviation was therefore explored to see if a representative RON value for JET A-1 had ever been determined, however no values had been derived as it is not relevant for the normal use of JET A-1 in turbine engines. However, using correlations derived by Kalghatgi (2005) a potential value for RON of 58.6 has been calculated for a cetane value of 30. This RON value was therefore used in the WAVE models developed using JET A-1 in order to determine if knock was predicted to be occurring. Knock was observed at lower full load engine speeds during the model runs. This could be observed occasionally at 2000 RPM and more so at 1000 RPM in terms of increased knock intensity. For speeds from 3000 RPM and above, no knock was observed.

Figures 13 and 14 present WAVE modelled predictions of cylinder pressure and torque for auxiliary port injection of JET A-1 for the key compression ratios respectively. As for Figures 9 and 10 the data is at 6000 RPM.

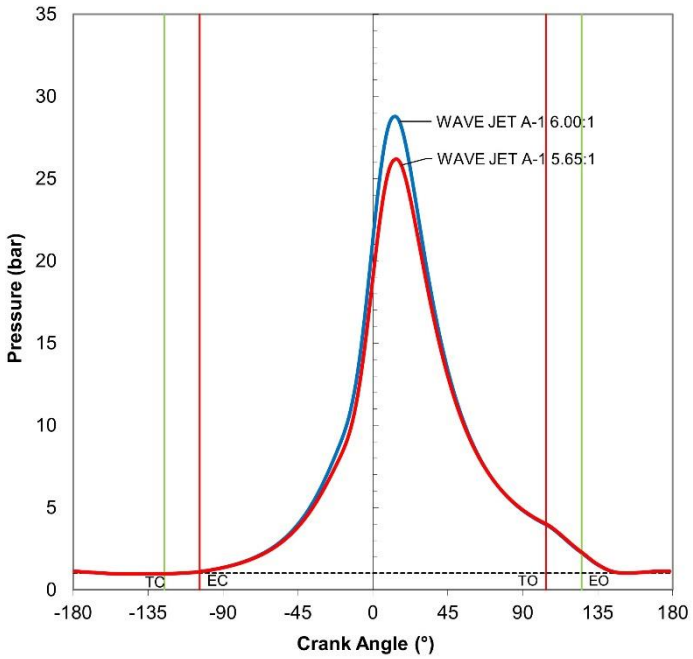

Figure 13. Comparison of cylinder pressures with WAVE modelled Auxiliary port fuel injection of JET A-1 with reduced 6.00:1 (8.02:1) and 5.65:1 (7.28:1) TCR at 6000 RPM

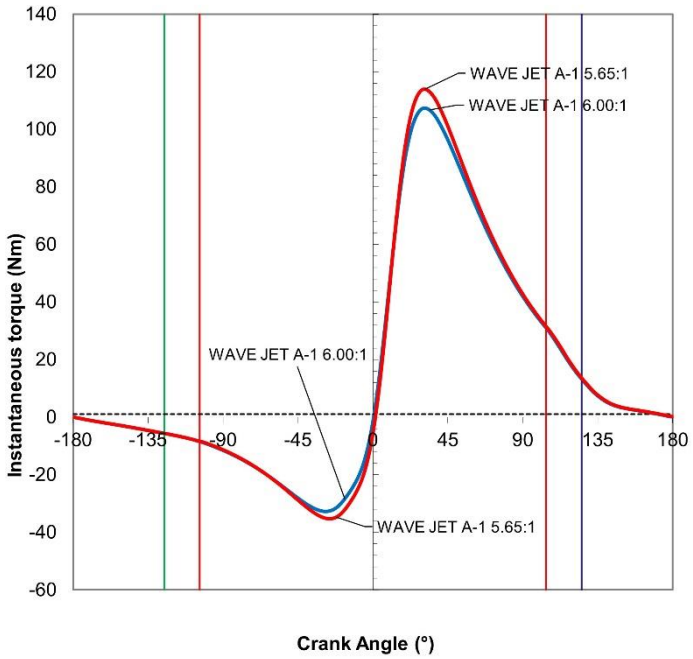

Figure 14. Comparison of instantaneous torque predictions with WAVE modelled Auxiliary port fuel injection of JET A-1 with reduced 6.00:1 (8.02:1) and 5.65:1 (7.28:1) TCR at 6000 RPM

In Figure 13 the maximum cylinder pressure using 6.00:1 TCR is 28.8 bar occurring at 13.1° ATDC. Reducing the TCR to 5.65:1 shows a predicted maximum cylinder pressure of 26.2 bar at 14.1° ATDC. Close examination of the rate of rise of pressure in Figure 13 shows a more rapid increase before TDC and therefore greater compression work for the higher 6.00:1 compression ratio. There is a less pronounced increase in expansion work after TDC. The predicted torque shown in Figure 14 shows a peak positive torque of 107.4 Nm with a TCR of 6.00:1 and a corresponding peak negative of -32.7 Nm. Reducing the TCR to 5.65:1 predicts peak torque values of 113.9 Nm and -35.3 Nm respectively.

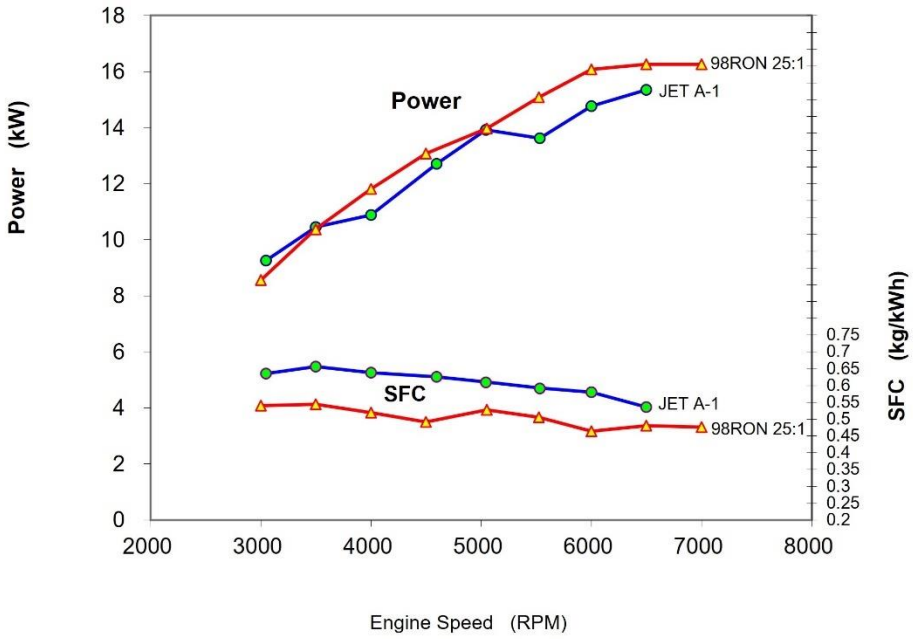

Figure 15. Dynamometer experimental performance comparison of kerosene JET A-1 with carburetted gasoline (98RON 25:1) oil premix fuel

On reference to Figure 15, it can be seen that the experimental recorded power at 5000 RPM is identical with both fuels, however the SFC is increased to 0.593 kg/kWh with kerosene from 0.528 kg/kWh with 25:1 98 RON gasoline/oil mixture. At 7000RPM it was not possible to operate effectively without running into excessive knock using kerosene JET A-1. Testing was therefore limited to a maximum of 6500 RPM.

The density range of the Jet A-1 fuel used for all experimental testing of the subject engine was 792.9 - 799.9 kg/m^3 (measured at 15°C).

All experimental test data recorded from the test engine has been corrected for International Standard Atmospheric conditions (SAE, 2011).

Discussion

The research presented in this paper has considered the application of a simple low mass fuel injection system to a conventional UAV engine. This was done to explore the possibilities of achieving an acceptable outcome meeting the single fuel objectives for military engine powered systems. The effects of introduction of JET A-1 into the cylinder during the open cycle phase around bottom dead centre has achieved some promising results, following compression ratio reduction to avoid combustion knock occurrence and permit advancement of ignition timing to counter what would otherwise be significant performance degradation from the gasoline baseline test data. WAVE modelling exhibited higher occurrence of knock at speeds below 3000 RPM as indeed did the experimental engine on the dynamometer. However due to propeller power plant matching, the engine would not be able to operate at such low speeds at full load in a UAV installation. In practical terms such knock limitations could therefore be avoided.

Baseline testing of the standard gasoline engine with carburettor fuelling established the benchmark for computational modelling of the original engine and dynamometer experimentation with JET A-1 fuelling. The standard gasoline results indicated maximum power of 16.27 kW at 6500 RPM. The inlet injected model correlated closely at 4500-5000 RPM but displayed higher power levels below 4500 RPM. Above 5000 RPM the predicted power output from the model was significantly lower than the actual power output from the test engine of the order of 8.2 to 13.3%, the greatest deviation occurring at 6000 RPM. In terms of SFC, correlation was close below 4500 RPM but deviates from 4500 RPM and above.

Using auxiliary port injection of indolene the results showed a closer correlation at higher speeds in terms of power but less so in terms of SFC. WAVE modelling of auxiliary port injected JET A-1 showed corresponding maximum power predictions of 13.04 kW and 12.58 kW at 6000 RPM using 6.00:1 and 5.65:1 TCR respectively. The modelled SFC using API indicated minimum values of 0.656 kg/kWh and 0.677 kg/kWh at 4500 RPM for 6.00:1 and 5.65:1 TCR respectively. Further work could be conducted to provide a closer correlation of engine friction mean effective pressure within the engine models. Future work to secure data via Morse tests could be incorporated in the WAVE models. This was not possible within the current study. All modelling was therefore conducted with typical values associated with crankcase scavenged two-stroke cycle engines. Dynamometer test data, using JET A-1 delivery via auxiliary port injection, led to a maximum power of 14.19 kW using 6.00:1 TCR. This was observed at a maximum test speed of 6100 RPM with a corresponding SFC of 0.605 kg/kWh. Test speeds above 6100 RPM were not possible due to instability and detonation onset. Reducing the TCR to 5.65:1 allowed operation of the engine at full ignition advance levels typically associated with those achieved with gasoline fuel operation. This allowed a maximum power of 15.35 kW at 6500 RPM with a corresponding SFC of 0.536 kg/kWh to be recorded compared with 16.27 kW and 0.481 kg/kWh at the same speed using gasoline. By reducing the compression ratio a small power increase has been observed at lower engine speeds of 3000 RPM and 3500 RPM when operating on kerosene JET A-1, however at the design maximum power speed, a power loss of the order of 5.7% was apparent.

In terms of thermal efficiency, gasoline offers higher levels due to an ability to operate at lower SFC than has so far been possible operating the engine on kerosene JET A-1. At maximum power the increase in SFC was of the order of 11.4%. The orientation of the engine exhaust ports, directly opposite the auxiliary transfer port, is not ideal for maximising thermal efficiency. For all API models and dynamometer engine tests fuel was introduced as the port opens into the cylinder. The possibility for fuel short-circuiting directly to the exhaust port is a strong possibility with this arrangement and can therefore lead to high specific fuel consumption if the incoming air charge or exiting exhaust gases carries the fuel into the exhaust. Similarly the momentum of the delivered fuel particles can also potentially carry them into the exhaust without any contribution to the

combustion process. Notwithstanding these possibilities, it should also be noted that for the same operating conditions in terms of power and fuel volumetric flow, the specific fuel consumption using kerosene would be higher than that for gasoline due to the higher relative density of kerosene fuel. For this reason alone, operation on kerosene will suffer a 6.6% increase by virtue of its increased density compared with gasoline if volumetric flow rates remain identical.

Applying fuel injection to a crankcase scavenged two-stroke cycle engine, such as the engine used here, requires a fundamental change to the lubrication system. The subject engine used has been previously fuel injected via the inlet tract when applied to the BAE Systems Phoenix UAV system. This method of fuelling can retain the oil-in-fuel lubrication method, however; if the fuel is to be supplied further downstream within the engine, either via the transfer ports as in this study or via direct injection into the combustion chamber, then a separate precision metering pump and lubricant reservoir is required. The overall power plant mass increase with the additional fuel injection hardware therefore also has to allow for the addition of the separate lubrication system and reservoir to provide sufficient lubricant for the duration of a long endurance mission.

It should be pointed out that this type of lubrication system, commonly developed for two-stroke engine motorcycles, has to be applied to Wankel rotary combustion engines, however they are fuelled. It is therefore not a major disadvantage when compared with competing UAV engine types but it does erode some of the simplicity and minimal power plant system volume that a two-stroke cycle engine offers. There are alternatives to this addition to the crankcase scavenged engine whilst retaining the inherent advantages of a two-stroke operating cycle. If the scavenging system is segregated as demonstrated by the prior research of Hooper *et al* (2011) and Stone (2012). This type of engine utilises twin diameter or stepped pistons enabling complete separation of the crankcase and hence the lubrication system. These engines never have to operate with oil in the fuel and allow an isolated lubrication system to be located within the lower section of the engine as is common practice in four-stroke cycle engines.

Computational modelling of the experimental engine within the environment of Ricardo WAVE has provided interesting support and further exploration of the experimental test experience. WAVE is extensively used for the simulation of poppet valve four-stroke engines but is not well known for simulation of crankcase scavenged two-stroke engines and various adaptations have been required in order to successfully simulate the engine within the one-dimensional code.

Conclusions

Fluid dynamic modelling of a twin cylinder 342 cm^3 crankcase scavenged two-stroke cycle engine in support of dynamometer experimental testing using gasoline and JET A-1 kerosene fuels has been conducted to explore validation of the computational models with particular focus on the effects of trapped compression ratio. Whilst it was possible to operate the test engine on JET A-1 at lower speeds without physical adjustment to the TCR this was only possible after significantly retarding the ignition timing to avoid the onset of detonation. The retardation therefore severely reduced engine performance from the baseline gasoline results. Reducing the TCR enabled full ignition advance to be re-applied without the engine suffering from detonation problems. Following optimisation of the trapped compression ratio, the maximum power recorded using JET A-1 from the experimental engine was 15.35 kW at 6500 RPM with a corresponding specific fuel consumption of 0.536 kg/kWh equating to a power loss of 5.7% and an increase in SFC of 11.4% from standard gasoline performance levels. Corresponding maximum power from the same TCR models was 12.58 kW at 6000 RPM. Computational modelling demonstrated reasonable correlation particularly a lower engine speeds but less so at high speeds. The models are considered a good basis for future development to further improve their correlation with additional future experimental experience. Delivery of JET A-1 via the auxiliary transfer ports offers a lower cost alternative to direct injection methods, however the possibility for fuel short-circuiting is greater with this methodology than for direct in-cylinder injection approaches. Greater thermal efficiency is therefore possible with direct injection which has to be considered together when the overall fuel system mass increase is assessed. Direct injection normally requires higher fuel pressures which by necessity increases the mass of fuel pumps, injectors and associated hardware.

Acknowledgements

The support provided by Ricardo for the provision of WAVE is gratefully acknowledged by the author enabling the simulations performed during the study reported in this paper.

References

Austin, R (2010) – “Aircraft Systems – UAS Design, Development and Deployment” (Wiley International ISBN 978-0-470-05819-0 (2010))

Blank, D.A., Pouring, A.A., and Lu, J. (2001) - “Qualitative Flow Field Studies of Combustion in I.C. Engines Using a Simplified Sonex Bowl-in-Piston Geometry” (SAE Paper No. 2001-26-0021 (2001))

Bird, R.B., Stewart, W.E. and Lightfoot, E.N. (2002) - "Transport Phenomena" (2nd edition, Wiley, 2002)

Blair, G.P. (1996) - "Design and Simulation of Two-stroke Engines", (SAE International, Warrendale, Pennsylvania, 1996).

Blundell, D., Turner, J., Pearson, R., Patel, R. and Young, J. (2010) – “The Omnivore Wide-range Auto-Ignition Engine: Results to Date using 98RON Unleaded Gasoline and E85 Fuels” SAE Paper No. 2010-01-0846 (2010)

Chen, S. K. and Flynn, P. (1965) – “Development of a Compression Ignition Research Engine” (SAE Paper No. 650733, 1965)

Davis, E.E. (1991a) – “Combat Tested/Combat Proven Unmanned Aerial Vehicles” (9th International RPV Conference, Bristol, 9-11 September 1991)

Douaud, A. M. and P. Eyzat. (1978) – "Four-Octane-Number Method for Predicting the Anti-Knock Behaviour of Fuels and Engines" (SAE Paper 780080 (1978))

Duddy, B., Lee, J., Walluk, M., and Hallbach, D. (2011) - "Conversion of a Spark-Ignited Aircraft Engine to JP-8 Heavy Fuel for Use in Unmanned Aerial Vehicles," SAE Int. J. Engines 4(1):82-93, 2011, https://doi.org/10.4271/2011-01-0145.

Duret, P., Ecomard, A., and Audinet, M. (1988) – “A New Two-Stroke Engine with Compressed_Air Assisted Fuel Injection for High Efficiency Low Emissions Applications” SAE Paper No.880176 (SAE International Congress and Exposition, Detroit, Michigan Feb 1988)

Ghojel, J.I. (2010) - "Review of the development and applications of the Wiebe function: a tribute to the contribution of Ivan Wiebe to engine research" (IMechE International Journal of Engine Research Vol. 11, Issue 4, 2010) DOI: 10.1243/14680874JER06510

Goraj, Z. and Frydrychewicz, A. (2004) - ‘‘Development Approach of the PW-103. An Increased Reliability Male UAV Under the CAPECON Project within the V FR of EU" (Proceedings of the 24th International Conference of Aeronautical Sciences, Yokohama, Japan, 29 August - 3 September 2004)

Heywood, J.B. & Sher, E. (1999) – “The Two-Stroke Cycle Engine: It’s Development, Operation and Design” (Taylor and Francis / SAE International ISBN 0-7680-0323-7 (1999))

Hinds, E.T. (1978) - “Intake Flow Characteristics of a Two-Stroke Cycle Engine fitted with Reed Valves” (PhD Thesis, Queen’s University of Belfast, August 1978)

Hooper, B. and Favill, J.E. (1978) - “Modern stepped piston engines” (IMechE Paper No.C133/78 Design and Development of Small IC Engines Conference, 31 May - 2 June 1978)

Hooper, P.R. (2019) - “Low Noise, Vibration and Harshness Solutions for in-Line Three-Cylinder Range Extender and Hybrid Electric Vehicles.” (International Journal of Engine Research 2019). https://doi.org/10.1177/1468087419859084

Hooper, P. (2017a) - "Low Volatility Fuel Cold Start Experience with a Stepped Piston UAV Engine to Address Single Fuel Objectives," (SAE International Journal of Engines 10(4):2017. SAE Technical paper 2017-01-9283, DOI: 10.4271/2017-01-9283) <http://papers.sae.org/2017-01-9283/>

Hooper, P.R. (2017b) - "Experimental experience of cold starting a spark ignition UAV engine using low volatility fuel", (Aircraft Engineering and Aerospace Technology, Vol. 89 Iss: 1, pp.106 – 111)

DOI http://dx.doi.org/10.1108/AEAT-09-2014-0137

Hooper, P.R., and Al-Shemmeri, T. (2017c) - "Improved efficiency of an unmanned air vehicle IC engine using computational modelling and experimental verification", (Aircraft Engineering and Aerospace Technology, Vol. 89 Iss: 1, pp.184 – 192) DOI http://dx.doi.org/10.1108/AEAT-09-2015-0200

Hooper, P.R., Al-Shemmeri, T., and Goodwin, M.J. (2011) – "Advanced modern low emission two-stroke cycle engines" (Proceedings of the Institution of Mechanical Engineers, Part D: Journal of Automobile Engineering. Vol. 225 No.11, November 2011)

Hooper, P.R., Al-Shemmeri, T., and Goodwin, M.J. (2012) – "An experimental and analytical investigation of a multi-fuel stepped piston engine" (Journal of Applied Thermal Engineering April 2012) <http://dx.doi.org/10.1016/j.applthermaleng.2012.04.034>

Kalghatgi, G.T. (2005) – "Auto-ignition quality of practical fuels and implications for fuel requirements of future SI and HCCI engines" (SAE Paper No. 2005-01-0239 (2005))

Kalkstein, J., Röver, W., Campbell, B., Zhong, L., Huang, H., Ping Liu, J., Tatur, M., Geistert, A., and Tusinean, A. (2006) - "Opposed Piston Opposed Cylinder (opoc™) 5/10 kW Heavy Fuel Engine for UAVs and APUs" (SAE Paper No. 2006-01-0278 SAE 2006 World Congress & Exhibition, Detroit April 2006)

Kucinski, W. (2018) - "So you want to Design Engines: UAV Propulsion Systems" (SAE International ISBN: 978-0-7680-9175-5)

Kweon, C. B. M. (2011) - "A Review of Heavy-Fueled Rotary Engine Combustion Technologies" (No. ARL-TR-5546. Army Research Laboratory Aberdeen Proving Ground MD.) < https://apps.dtic.mil/dtic/tr/fulltext/u2/a545309.pdf >

Liu, R., Wei, M., and Yang, H. (2016) - "Cold start control strategy for a two-stroke spark ignition diesel-fuelled engine with air-assisted direct injection" (Applied Thermal Engineering 108 (2016) pp414-426)

Liu, R., Wei, M., Wang, C., and Huang, T. (2019) - "Fuel Flow Control for Starting a Crankcase-Injected Two-Stroke Spark Ignition Engine Fueled with Kerosene (RP-3)" (Journal of Energy Engineering/Volume 145 Issue 4 - August 2019)

Malriat, J., Hill, W., Soimar, M and Christ, A. (1991b) – "Heavy Fuel Development for the Joint Unmanned Aerial Vehicle Program" (9th International RPV Conference, Bristol, 9-11 September 1991)

Mattarelli, E., Rinaldini, C., and Baldini, P. (2014) - "Modeling and Experimental Investigation of a 2-Stroke GDI Engine for Range Extender Applications," (SAE Technical Paper 2014-01-1672, (2014), doi:10.4271/2014-01-1672.)

McDonald, C.F., Massardo, A.F., Colin Rodgers, C., and Stone, A. (2008) - "Recuperated gas turbine aeroengines. Part III: engine concepts for reduced emissions, lower fuel consumption, and noise abatement" (Aircraft Engineering and Aerospace Technology, Vol. 80 No. 4, pp. 408-426) DOI: https://doi.org/10.1108/00022660810882773

Morrison, J.L.M. and Crossland, B. (1971) – "An Introduction to the Mechanics of Machines" (2nd Edition Longman, ISBN 978 0582447295 (1971))

Owens, E., LePera, M., and Lestz, S. (1989) - "Use of Aviation Turbine Fuel JP-8 as the Single Fuel on the Battlefield," SAE Technical Paper 892071, 1989, doi:10.4271/892071

Ricardo PLC website (2022) – WAVE simulation software information available from:- <https://software.ricardo.com/products/wave/wave-engine-performance> [accessed 14 April 2022]

SAE (2011) - "J1349 Engine power test code – spark ignition and compression ignition – net power rating" (Warrendale, Pennsylvania: SAE International, 2011)

Schlunke, K.(1989) – “The Orbital Combustion Process Engine” (10th Vienna Motorsymposium, VDI No. 122, pp63-68, 1989)

Schweitzer, P.H. (1949) – “Scavenging of Two-Stroke Diesel Engines” (The Macmillan Company, New York (1949))

Sher, E.(1984) – “The Effect of Atmospheric Conditions on the Performance of an Airborne Two-Stroke Spark Ignition Engine” (Proc. Inst. Mech. Eng., Part D, Vol 198, No. 15 pp 239-251, 1984)

Stone, R. (2012) - Introduction to Internal Combustion Engines, 4th Edition (Palgrave MacMillan) ISBN: 9781137028297 (2012)

Turan, O. (2012) - "Exergetic effects of some design parameters on the small turbojet engine for unmanned air vehicle applications" (Energy, The International Journal, 46 (2012), pp. 51-61)

Turner, J., Blundell, D., Pearson, R., Patel, R. Larkman, D., Burke P., Richardson, S., Green, N.M., Brewster, S., Kenny, R. and Kee, R. (2010) – “Project Omnivore: A Variable Compression Ratio ATAC 2-Stroke Engine for Ultra-Wide-Range HCCI Operation on a Variety of Fuels” SAE Paper No. 2010-01-1249 (2010)

US Department of Defense Directive 4130.43 (1988) - “Fuel Standardization,” Office of the Secretary of Defense, Washington, DC, 1988.

Wiebe, I. (1967) – “Halbempirische Formel für die Verbrennungsgeschwindigkeit” (Verlag der Akademie der Wissenschaften der UdSSR, Moscow, 1967)

Work, F (2011) - "Development of multi-fuel, power dense engines for maritime combat craft" (Journal of Marine Engineering & Technology, Vol 10 Issue 2, 37-46)

Woschni, G. (1967) – “A universally applicable equation for the instantaneous heat transfer coefficient in the Internal Combustion Engine” SAE Paper No.670931 (SAE Transactions., Vol 76, pp 3065, 1967)

Xu, Z., Ji, F., Ding, S., Zhao, Y., Zhou, Y., Zhang, Q., and Du, F. (2021) - "Digital twin-driven optimization of gas exchange system of 2-stroke heavy fuel aircraft engine" (Journal of Manufacturing Systems, Volume 58, Part B, January 2021, pp132-145) <https://doi.org/10.1016/j.jmsy.2020.08.002>

Zigler, B. T., Keros, P. E., Helleberg, K. B., Fatouraie, M., Assanis, D., and Wooldridge, M. S. (2011) - "An experimental investigation of the sensitivity of the ignition and combustion properties of a single-cylinder research engine to spark-assisted HCCI" (International Journal of Engine Research, 12(4), 353-375)

Nomenclature

Symbols

A	Cross sectional area
A_b	Reed bending plane cross sectional area
A/F	Air:fuel ratio
A_o	Open port area
A_p	Knock multiplier
A_r	Geometric open port area
A_T	Activation temperature multiplier
b	Constant
B_0	Frequency factor
c	Constant
$c_{1,2,3,4}$	Constants
C_d	Discharge coefficient
C_d	Flow coefficient

C_m	Relative heat transfer area scaling factor
c_p	Constant pressure specific heat
D	Cylinder diameter
D_R	Delivery ratio
E	Modulus of Elasticity
f_r	Reed natural frequency
f_t,	Burn scale post knock multiplier
h	Heat transfer coefficient
h_o	Port open height
I	Second moment of area
k_r	Reed spring constant
l_r	Reed length
$\dot{m}$	Mass flow rate
m_r	Reed mass (lift portion)
m_{liq}	Unburned liquid fuel mass
m_{vap}	Unburned fuel vapour mass
N	Engine speed
n_r	Number of reeds
O_N	Fuel research octane number
p_{cyl}	Cylinder pressure
p_f	Friction mean effective pressure
p_{max}	Maximum cylinder pressure
p_o	Upstream stagnation pressure
p_f	Friction mean effective pressure
p_{max}	Maximum cylinder pressure
p_r	Gas pressure at reference condition
p_R	Pressure at restriction
P	Instantaneous gas pressure
P_r	Prandtl number
P_w	Reed port width
r_c	Compression ratio
r_{cc}	Crankcase Compression Ratio
r_{cTrap}	Trapped compression ratio
R	Universal gas constant
r_p	Port corner radius
r_{tip}	Deflection at reed tip
s	Stroke
t_i	Start time of auto-ignition
t_o	Start time of end gas compression
t_r	Reed thickness
T	Instantaneous gas temperature
T_{act}	Activation temperature
T_{af}	Adiabatic flame temperature
T_o	Upstream stagnation temperature
T_{unb}	Temperature of the cylinder unburned gas fraction
w_p	Width of port
w_r	Reed petal width normal to flow
V_c	Clearance volume
V_{aEC}	Swept volume after exhaust port closure
v_{ch}	Characteristic gas velocity
$x(\theta)$	Mass fraction burned at crank angle θ
$\beta_j l_r$	Reed vibration mode
$\Delta\theta_b$	Duration of combustion
θ	Crank angle θ_0 Crank angle at start of combustion
θ_p	Reed open period
γ	Ratio of specific heats
τ	Ignition delay
τ_{post}	Post detonation burn time

Definitions, Acronyms and Abbreviations

API	Auxiliary Port Injection
AVTUR	AViation TURbine fuel
BDC	Bottom Dead Centre
BMEP	Brake Mean Effective Pressure
CCR	Crankcase Compression Ratio
DF-2	Diesel Fuel 2
DoD	United States Department of Defense
DI	Direct Injection
EXP	Dynamometer Experimental data
FMEP	Friction Mean Effective Pressure
HFE	Heavy Fuel Engine
II	Inlet Injection
JET A-1	Commercial aviation grade kerosene fuel
JP-5	Jet Propulsion 5 fuel
JP-8	Jet Propulsion 8 fuel
NATO	North Atlantic Treaty Organisation
RON	Research Octane Number
RPM	Revolutions per minute
SFC	Specific Fuel Consumption
SI	Spark Ignition
TCR	Trapped Compression Ratio
TDC	Top Dead Centre
UAV	Unmanned Air/Aerial Vehicle
UAS	Unmanned Air/Aerial System

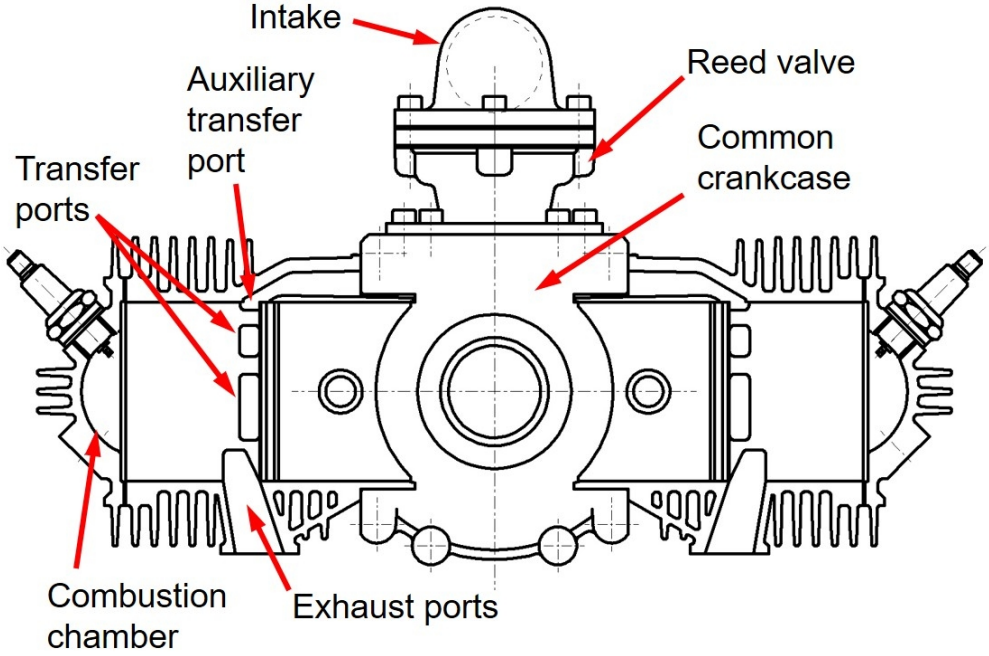

Figure 1. Engine sectional arrangement

187x129mm (150 x 150 DPI)

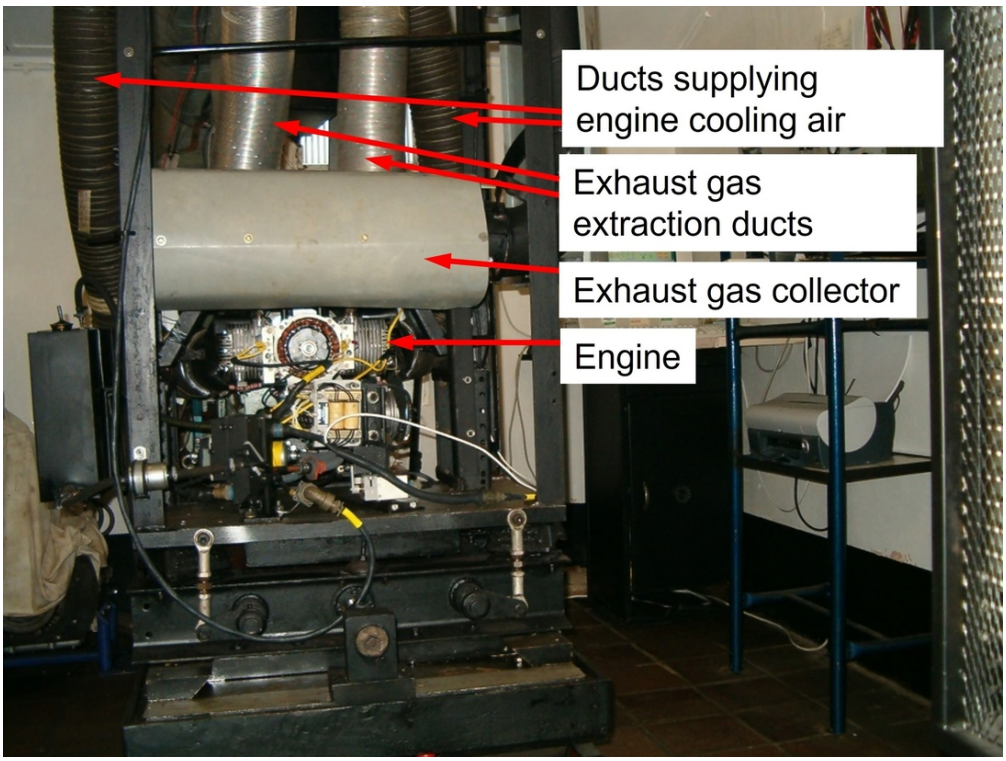

Figure 2. Engine dynamometer installation

184x138mm (150 x 150 DPI)

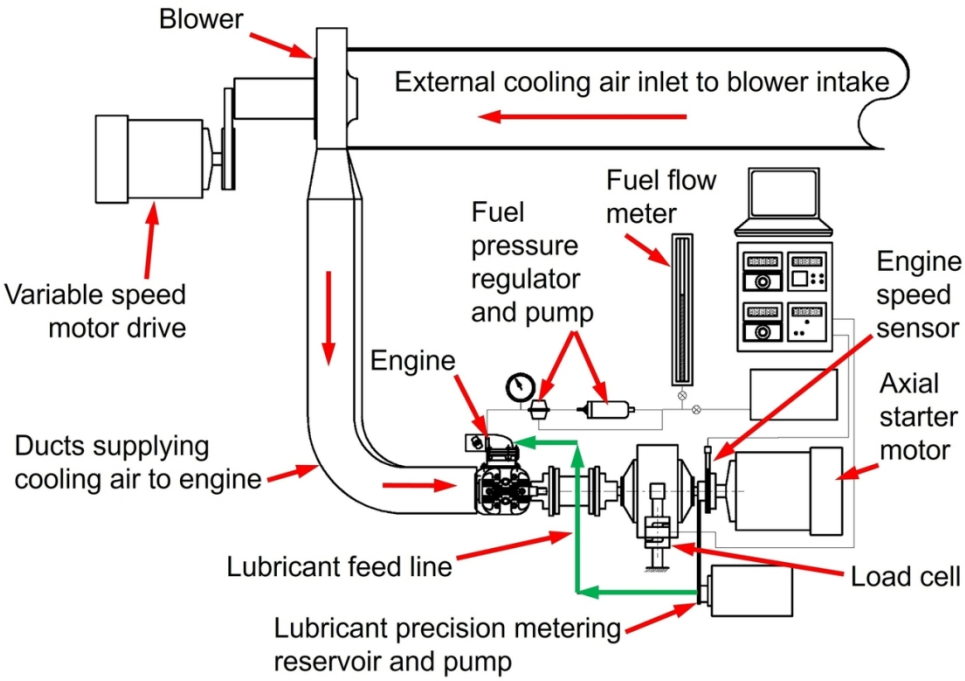

Figure 3. Engine dynamometer arrangement (Exhaust extraction system removed)

228x160mm (150 x 150 DPI)

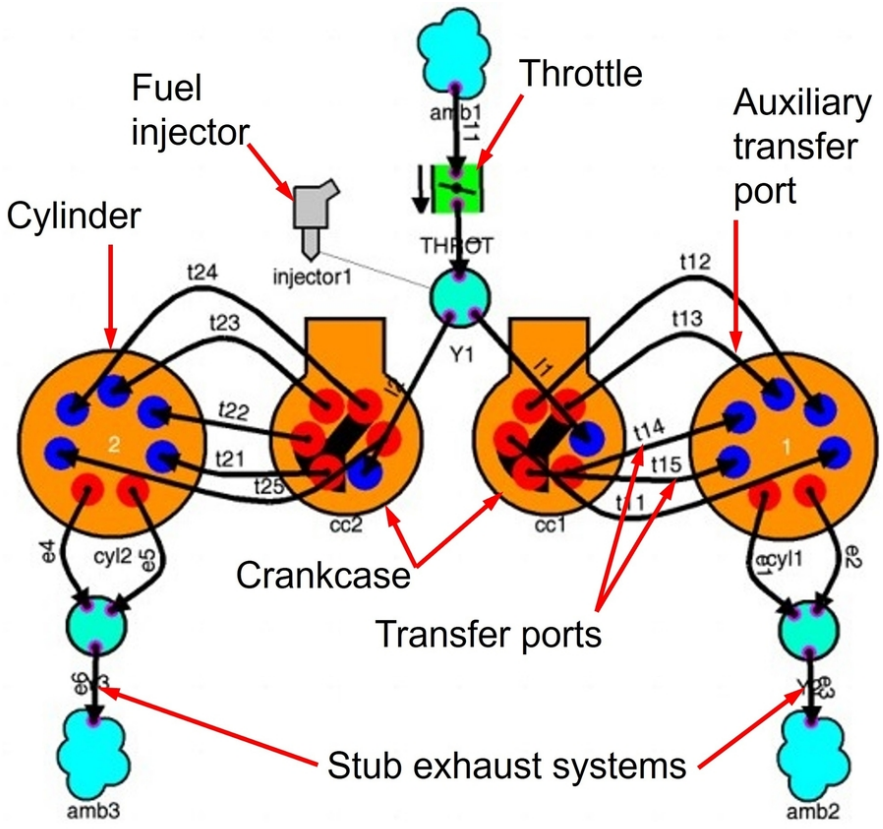

Figure 4. Engine one-dimensional model

172x147mm (150 x 150 DPI)

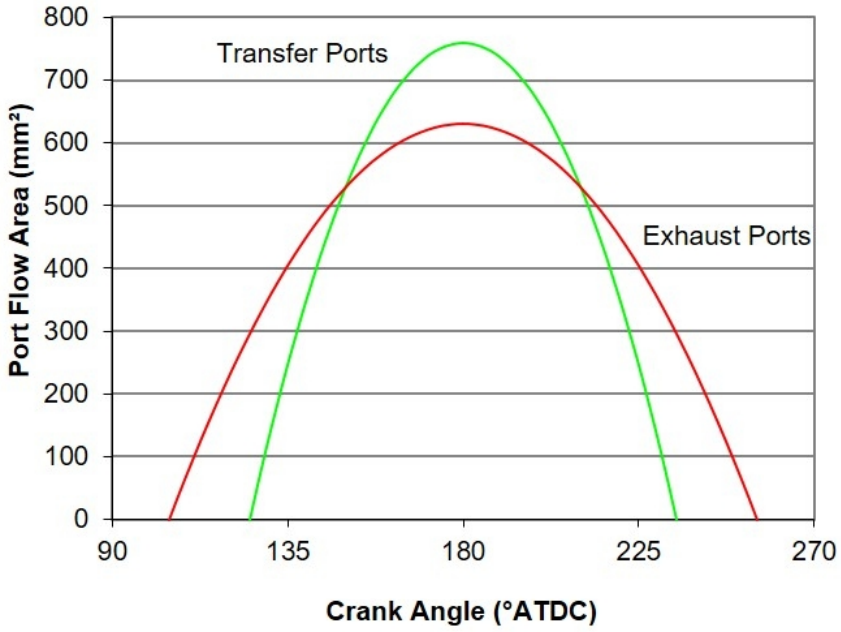

Figure 5. Port flow time - area history

129x96mm (150 x 150 DPI)

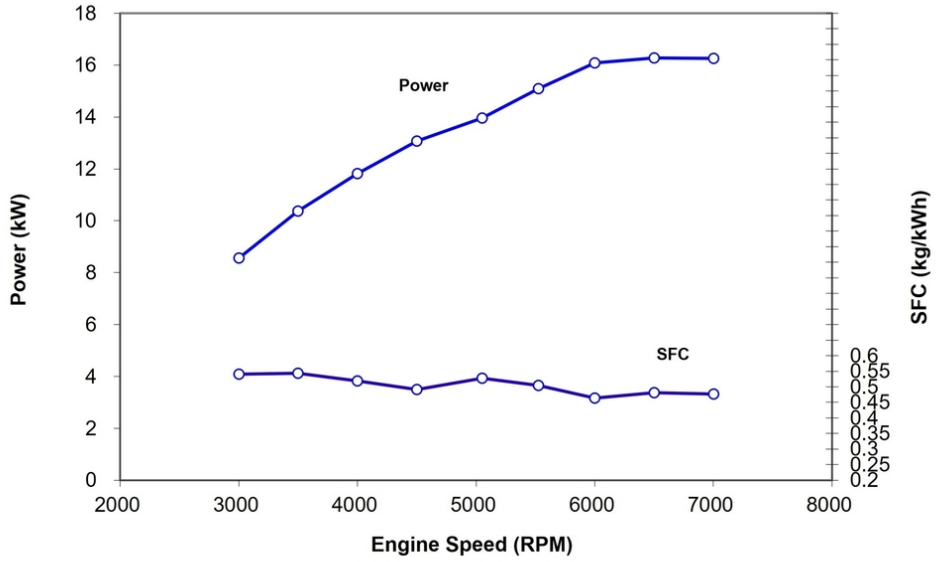

Figure 6. Initial experimental baseline test data of engine recorded using carburettor fuelling with 98RON gasoline with 25:1 oil premix

170x118mm (150 x 150 DPI)

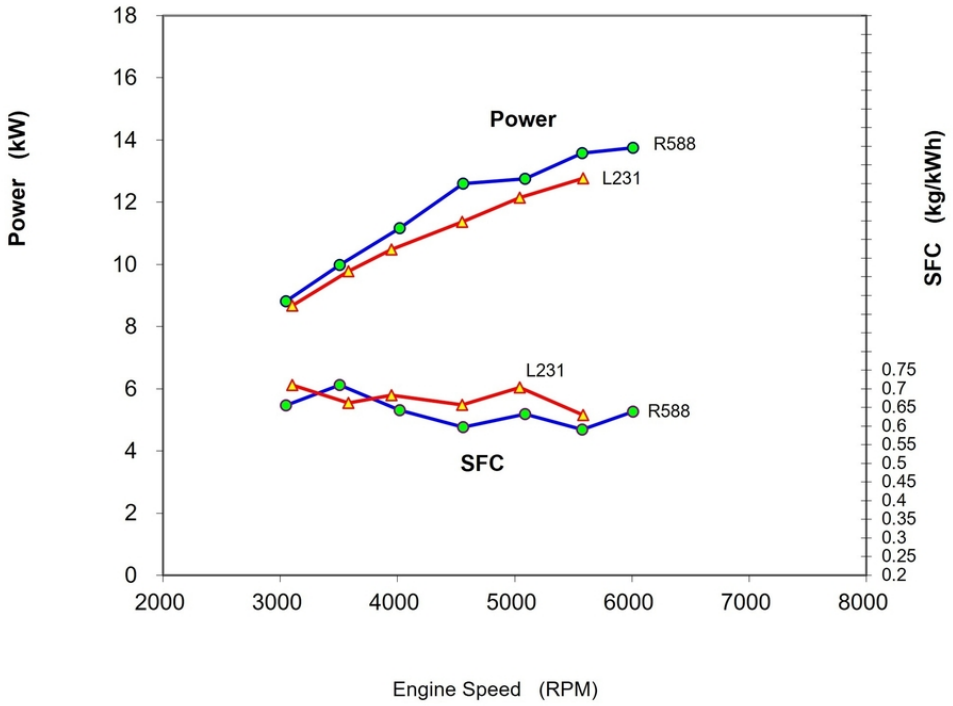

Figure 7. Comparison of experimental kerosene JET A-1 performance using high (R588) and low (L231) flow rate injectors

159x123mm (150 x 150 DPI)

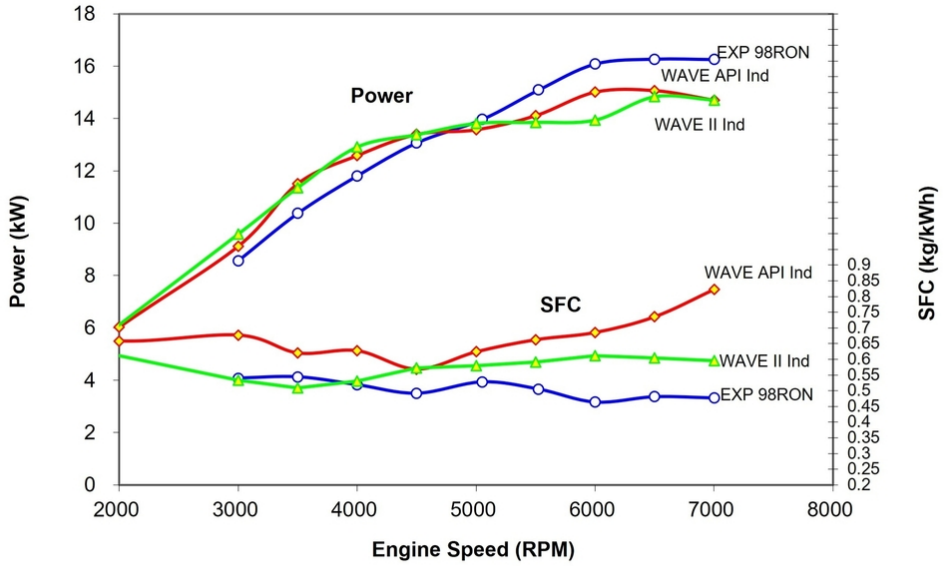

Figure 8. Comparison of 98RON gasoline experimental (EXP) data with WAVE modelled Auxiliary port injection (API) and inlet injection (II) of indolene

169x119mm (150 x 150 DPI)

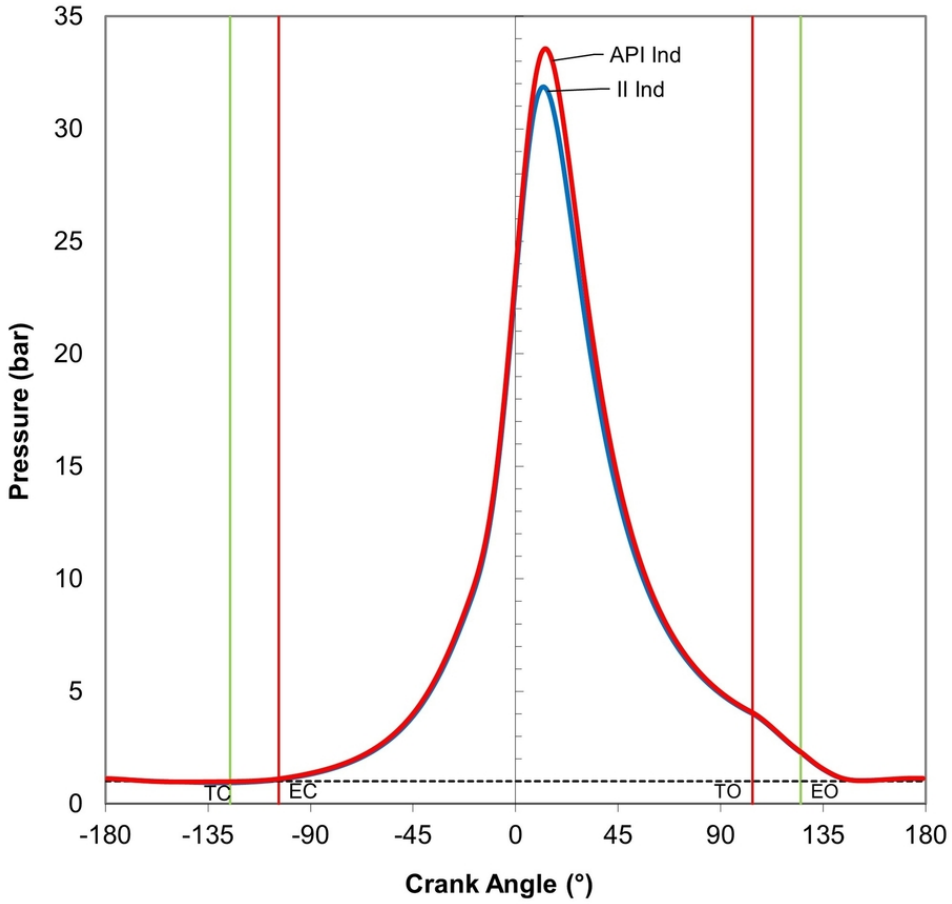

Figure 9. Comparison of cylinder pressures with WAVE modelled Auxiliary port injection (API) and inlet injection (II) of indolene at 6000 RPM

161x154mm (150 x 150 DPI)

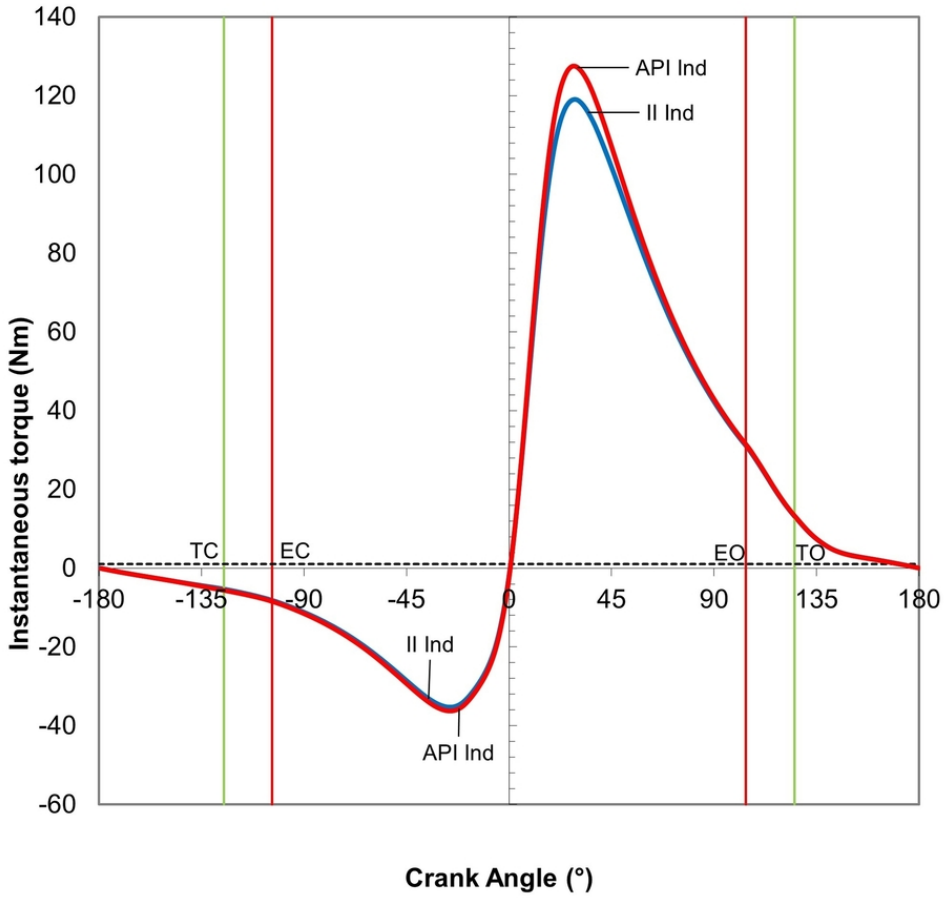

Figure 10. Comparison of instantaneous torque predictions with WAVE modelled Auxiliary port injection (API) and inlet injection (II) of indolene at 6000 RPM

161x154mm (150 x 150 DPI)

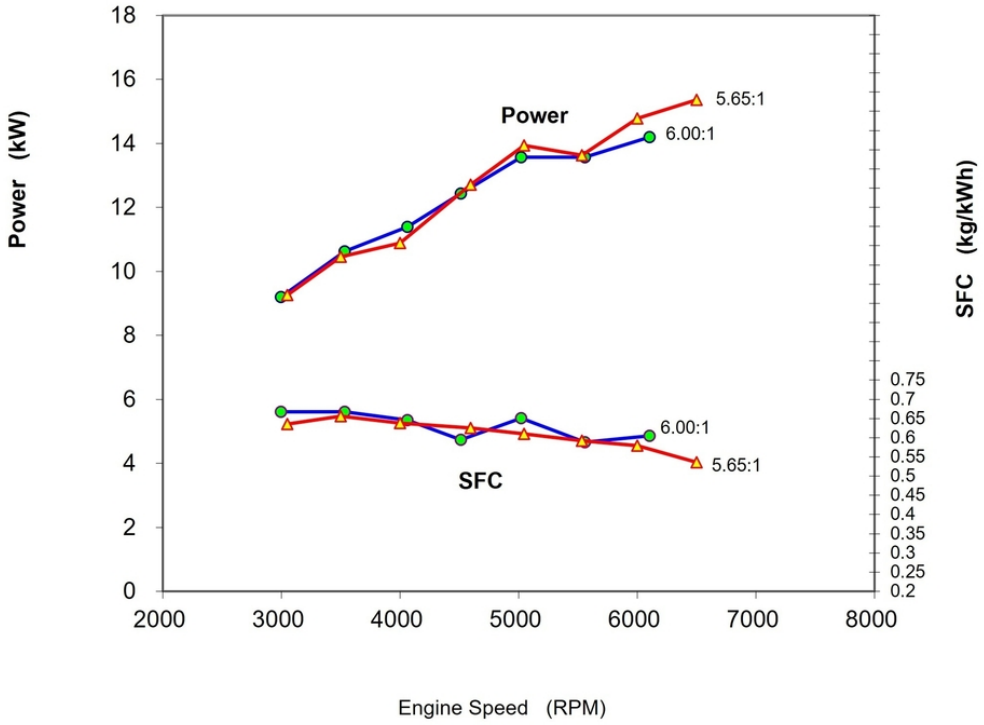

Figure 11. Dynamometer experimental comparison of kerosene JET A-1 injection using 6.00:1 and 5.65:1 trapped compression ratios

156x125mm (150 x 150 DPI)

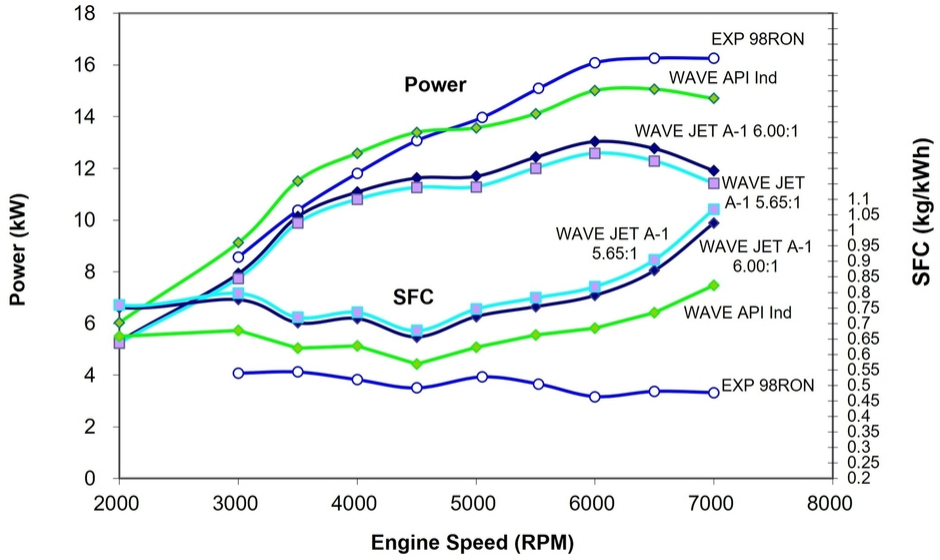

Figure 12. Effect of compression ratio using full compression 98RON gasoline experimental (EXP) data and WAVE modelled Auxiliary port fuel injection of JET A-1 with reduced 6.00:1 (8.02:1) and 5.65:1 (7.28:1) TCR

169x117mm (150 x 150 DPI)

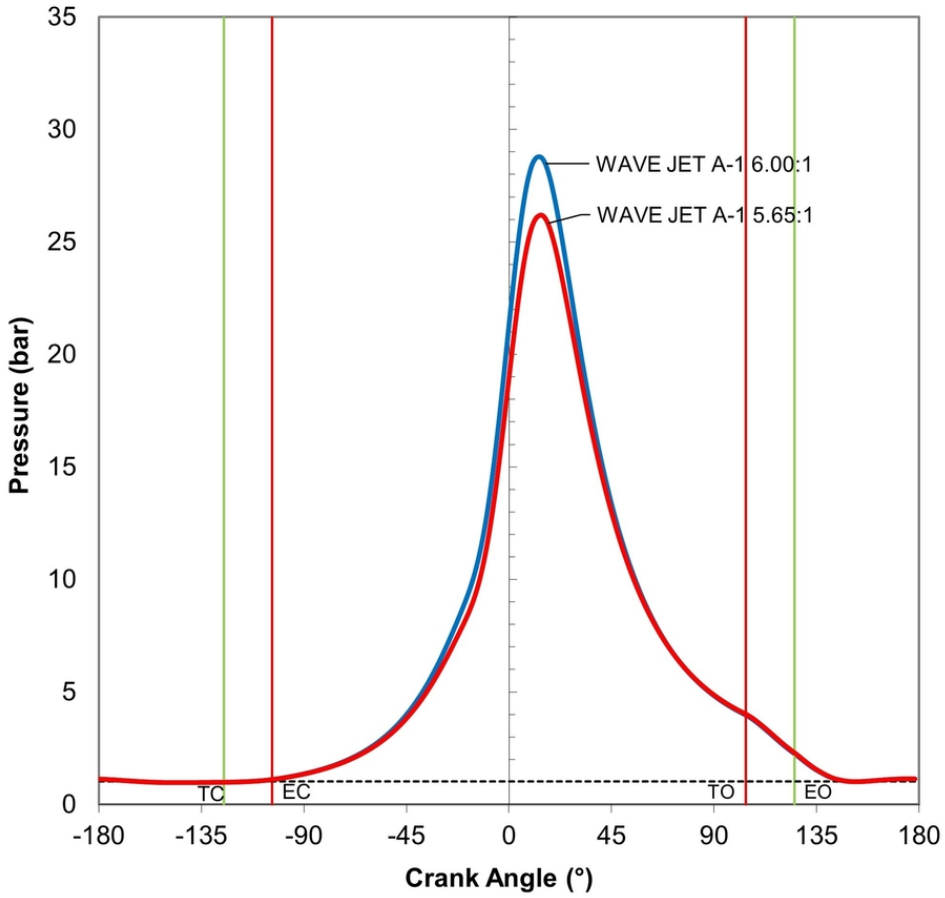

Figure 13. Comparison of cylinder pressures with WAVE modelled Auxiliary port fuel injection of JET A-1 with reduced 6.00:1 (8.02:1) and 5.65:1 (7.28:1) TCR at 6000 RPM

161x154mm (150 x 150 DPI)

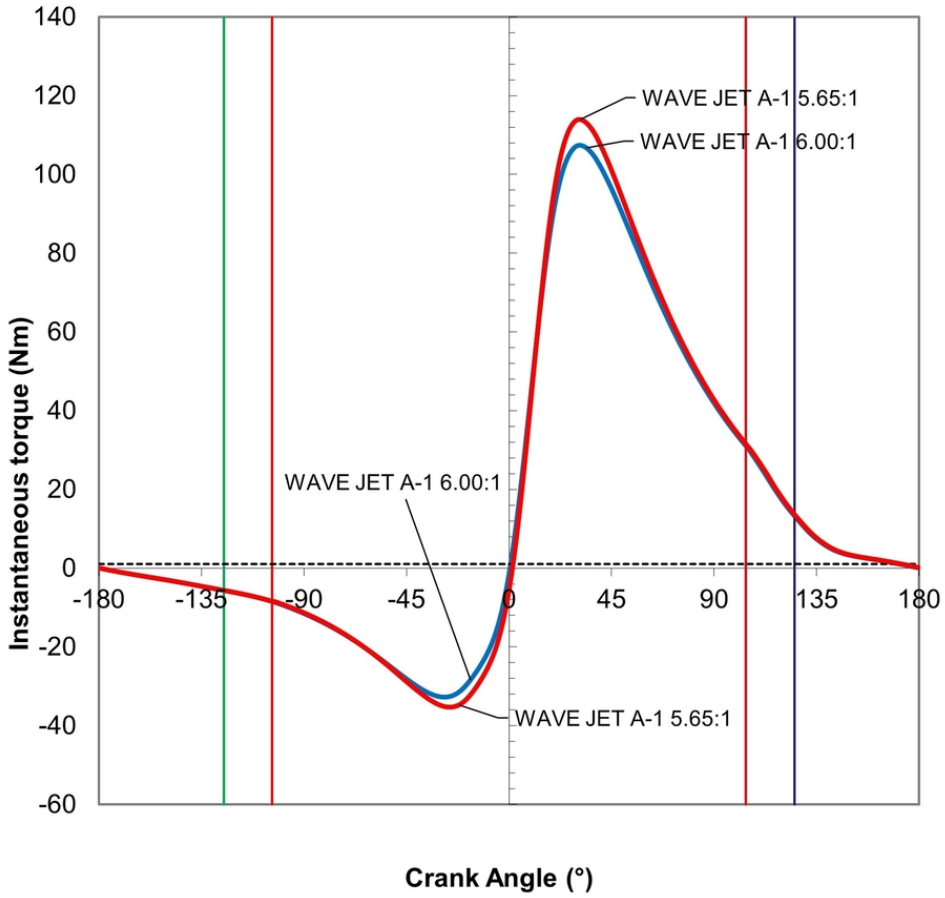

Figure 14. Comparison of instantaneous torque predictions with WAVE modelled Auxiliary port fuel injection of JET A-1 with reduced 6.00:1 (8.02:1) and 5.65:1 (7.28:1) TCR at 6000 RPM

161x154mm (150 x 150 DPI)

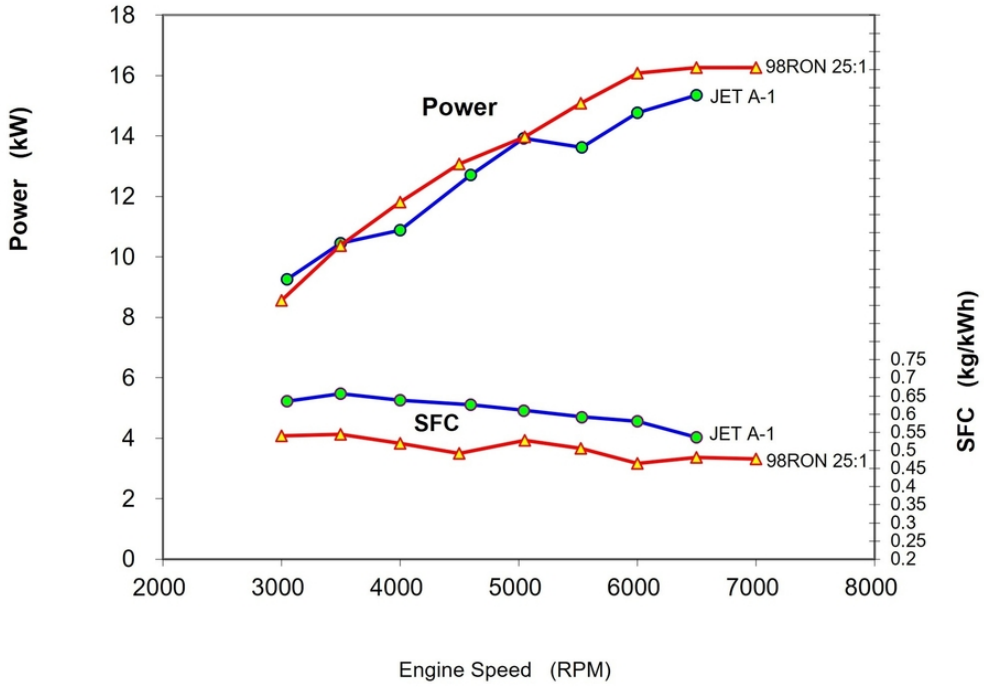

Figure 15. Dynamometer experimental performance comparison of kerosene JET A-1 with carburetted gasoline (98RON 25:1) oil premix fuel

153x115mm (150 x 150 DPI)

Table.1. Standard engine design data

Swept Volume (cm^3)	342
No. of cylinders	2
Bore (mm)	66
Stroke (mm)	50
Trapped compression ratio (r_{cTrap})	7.1:1
Crankcase compression ratio (r_{cc})	1.5:1
Induction control	Single 6 petal reed valve (steel reeds)
Fuel system	Single diaphragm carburettor
Alternative fuel system	Single point inlet injection upstream of the crankcase
Fuel	Gasoline (with 4% SAE40 two-stroke oil added)
Lubrication system	Total loss (Premixed fuel)
Exhaust system	Short stub pipes

Table 2. Port Open time and injector pulse width

Engine speed (rpm)	Port Open Time (ms)	L231 injector pulse width (ms)	R588 injector pulse width (ms)
3000	5.50	4.05	3.51
3500	4.71	3.85	3.57
4000	4.13	3.87	3.00
4500	3.67	3.56	2.83
5000	3.30	3.55	2.63
5500	3.00	3.33	2.57
6000	2.75		2.52
6500	2.54		
7000	2.36		

Table 3. Experimental full geometric and trapped compression ratios

Full geometric compression ratio (r_c)	Trapped compression ratio (r_{cTrap})
9.20:1	6.74:1
8.02:1	6.00:1
7.28:1	5.65:1

Study of the effects of trapped compression ratio on the heavy fuel operation of a spark ignition Unmanned Aerial Vehicle engine

Abstract

Purpose – This paper aims to present experimental experience of heavy fuelling of a spark ignition crankcase scavenged two-stroke cycle Unmanned Aerial Vehicle engine, particularly focusing on the effects of compression ratio variation and to cross correlate with the results of fluid dynamic modelling of the engine and fuels used.

Design/methodology/approach – One-dimensional modelling of the engine has been conducted using WAVE software supported by experimental dynamometer testing of a spark ignition UAV engine to construct a validated computational model using gasoline and kerosene JET A-1 fuels.

Findings – The investigation into the effects of compression ratio variation via fluid dynamic simulation and experimental testing has allowed an assessment of the approach for improving heavy fuel operation of UAV engines using auxiliary transfer port fuel injection. The power level achieved with reduced compression ratio heavy fuel operation is equal to 15.35 kW at 6500 RPM compared to 16.27 kW from the standard gasoline engine or a reduction of 5.7%.

Practical implications – The studied engine is specifically designed for UAV applications. The validation of the computational models to explore the effects of compression ratio and heavy fuel injection on the solution and cost is supported by experimental tests.

Originality/value – The application of auxiliary port fuel injection of heavy fuel and associated compression ratio optimisation offers an alternative approach to achieve the safety and logistical challenges of the single fuel policy for UAVs. The application of WAVE to simulate crankcase scavenged two-stroke cycle engines has been applied in very few cases. This study shows further exploratory work in that context.

Keywords *Heavy fuel engine, JET A-1, kerosene spark ignition, engine modelling, internal combustion engine, two-stroke cycle engine, UAV engine, UAS engine.*

Paper type Research paper

Introduction

The single fuel policy (US DoD (1988)) as discussed by Owens *et al* (1989) has to some extent been successfully implemented for some elements of military equipment, however; key areas still remain a challenge as discussed by Duddy *et al* (2011) and Hooper (2017a). Unmanned Aerial Systems (UAS) or unmanned aerial vehicles (UAV) are such an area. The majority of systems operating at medium to low altitude are predominantly systems operating with gasoline fuelled internal combustion engines as demonstrated by the AAI Shadow RQ-7, Elbit Hermes 450/Thales Watchkeeper, IAI Heron and General Atomics MQ-1 air vehicles (Austin, 2010). Gasoline is a readily available fuel providing good performance levels, however; in a military theatre of operations its use presents major logistical and safe operational problems as discussed by Davis (1991) and Malriat *et al* (1991). Several engine research programmes have explored adaptation of pre-existing UAV engines using four-stroke cycle and two-stroke cycle power plants as indicated by the research of Xu *et al* (2021) and the Ricardo Wolverine 3 engine as discussed by Liu *et al* (2019). These programmes have included conventional reciprocating piston technology as demonstrated by the work of Blank *et al* (2001) and Duddy *et al* (2011). Wankel rotary engines, which operate on a four-stroke cycle, have also been considered as reported by Kweon (2011) and Kucinski (2018). Four-stroke compression ignition diesel engines have seen some successful introduction into larger aircraft as indicated by the research of Goraj and Frydrychewicz (2004). Four-stroke engines, with the same number of cylinders, exhibit significantly inferior vibration characteristics than two-stroke engines as discussed by Hooper (2019). Some studies have considered unconventional technologies to successfully address the challenge as demonstrated by the research of Kalkstein (2006) using opposed piston engine technology and that of Hooper *et al* (2012) building upon the prior research work of Hooper and Favill (1978) with segregated scavenging for higher durability.

Turbine engines have also been considered for smaller UAVs as demonstrated by the work of Turan (2012) and McDonald *et al* (2008) with some success. Turbines are perhaps better suited to operate on low volatility fuels and are designed to function most efficiently on such fuels, however; for UAV application their loiter speeds can be a limiting factor unless a rotary wing solution is adopted. Piston engine UAVs are more readily suited for slower loitering speeds over a designated target position. The high specific fuel consumption of small turbines is also a limiting factor in their application to small air vehicles.

The low volatility fuels considered for UAVs include kerosene-based fuels such as JP-5, JP-8, AVTUR and JET A-1 and diesel fuels such as DF2. The fuel forming the feed stock in this study is kerosene JET A-1. All of these fuels present advantages over gasoline in terms of safer storage and supply, a key benefit when having to move fuel to forward operating positions. A further advantage is in terms of logistics. The only military systems requiring gasoline was motorcycles, light all-terrain vehicles, outboard motors and UAVs. Research and development has successfully resolved or provided potential solutions to all but the UAV application as presented by Work (2011). For this reason, gasoline is naturally seen as a seriously problematic fuel requiring special treatment especially onboard Navy vessels with contingency plans in place to jettison the stock in cases of emergency.

By the very nature of the fuels considered so far, their low volatility presents serious challenges in terms of achieving cold starting, acceptable levels of operational performance and avoiding the onset of combustion knock or detonation in spark ignition engines. Cold starting has been demonstrated to be achievable via the research of Hooper (2017a), Hooper and Al-Shemmeri (2017b) and Liu *et al* (2016). Achieving good performance levels whilst avoiding detonation is essential. Combustion knock will destroy an internal combustion engine. Continued operation in conditions provoking the onset of knock can result in an avalanche effect resulting in localised overheating of critical exposed areas of pistons, combustion chamber surfaces and premature bearing failure due to the higher loading experienced by the small end bearing in particular.

Significant difficulties in terms of detonation naturally exist for Wankel type rotary combustion engines due to the shape of the combustion chamber. The inherently long flame path, usually inevitable with rotary combustion engine arrangements, leads to heightened susceptibility to the engine type suffering from combustion knock occurrence. This is a consequence of the unavoidably long distances to the cool end gas location with the rectangular profile of the chamber section. Detonation can also be a major problem for conventional piston engines but it is often easier to design the engine to secure a relatively short flame path to the extremities of the chamber.

The most effective fuelling system in terms of maximising thermal efficiency for a two-stroke cycle engine has largely been demonstrated by adoption of direct injection as shown by the research of Duret (1988), Schlunke (2001) and more recently by Turner *et al* (2010), Blundell *et al* (2010) and discussed by Hooper *et al* (2011, 2012) and Stone (2012). More recently Matarelli *et al* (2014) have discussed concepts of applying DI to two-stroke engines for automotive application. Unfortunately, direct injection hardware suffers a greater mass penalty when compared with low pressure fuel injection systems delivering fuel via the inlet port or further upstream via the transfer ports. This penalty is due to the nature of the combustion pressure/heat exposure of the injectors and that higher fuel delivery pressures are normally required for DI. This is of course offset to an extent by the lower fuel payload secured by the increased thermal efficiency but nevertheless a trade off becomes apparent for the UAV system integration adopted.

This paper focuses on application of low-pressure fuel injection of kerosene JET A-1 into the transfer port area of a two-stroke cycle UAV engine to assess the feasibility of operation of the engine on heavy fuel. Experimental testing of the engine and further supporting modelling of the engine using proprietary well respected engine simulation software in order to simulate engine modifications and explore correlation between the real and virtual engines.

Methodology

A twin cylinder 342 cm^3 crankcase scavenged two-stroke engine was used for this study. The basic form of the engine uses a single diaphragm carburettor supplying a common crankcase. The engine was therefore modified to allow installation of low-pressure auxiliary port injection (API). A cross-sectional arrangement of the engine arrangement is shown for reference in Figure 1.

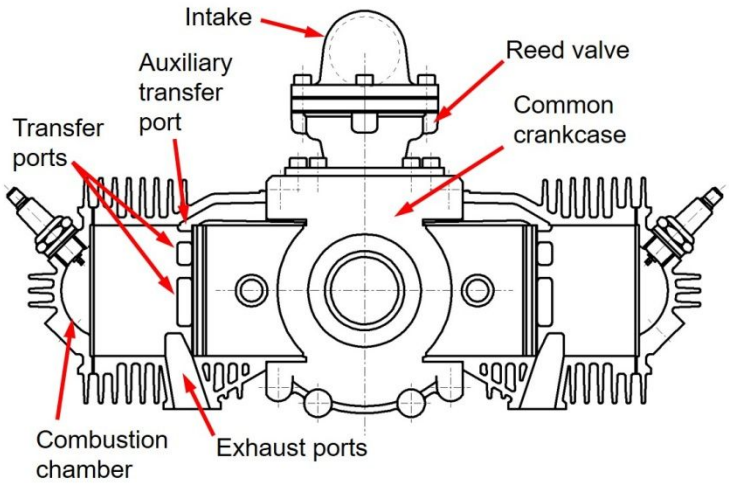

Figure 1. Engine sectional arrangement

As can be seen in Figure 1, the engine is a 180° horizontal flat-twin design and employs a shared crankcase providing scavenge air for both cylinders. Each cylinder of the engine displaces a swept volume of 171 cm^3.

The dynamometer installation of the engine can be seen in Figure 2.

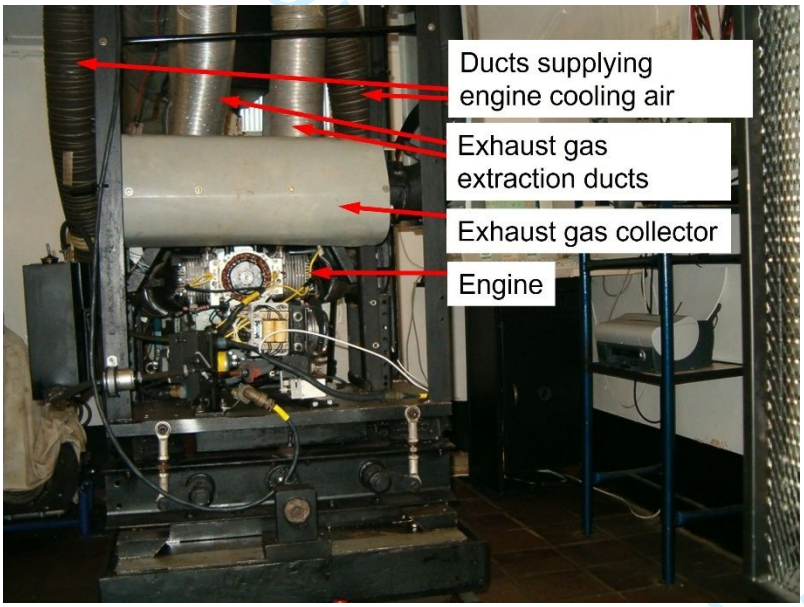

Figure 2. Engine dynamometer installation

Cooling air was ducted to the engine via flexible ducts to each individual cylinder. The air being supplied via a variable speed centrifugal blower with air ducted to the blower intake from outside the test cell. The standard engine was originally designed to operate with short stub exhaust pipes. In order to accommodate the same system for experimental testing an exhaust gas collector/muffler was fabricated and positioned close to the engine in order to collect and safely extract exhaust gases out of the test cell. A schematic of the test cell arrangement providing more details of the experimental test installation is shown in Figure 3.

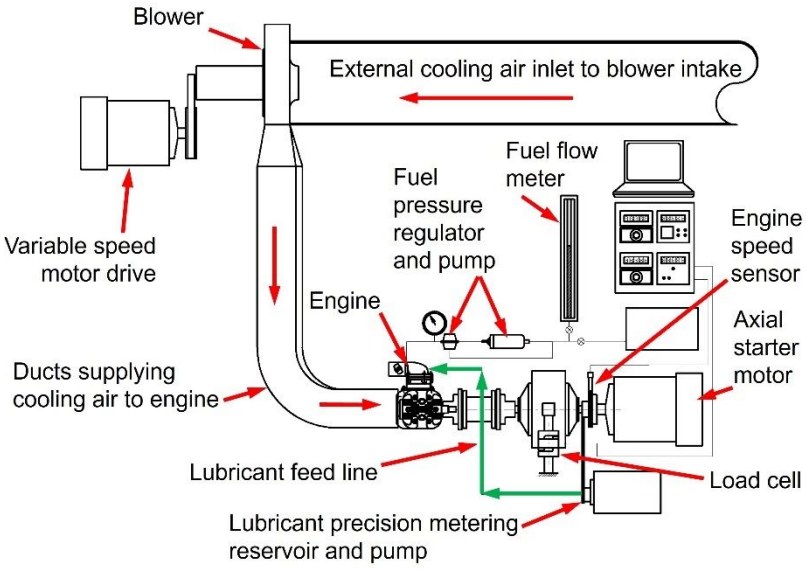

Figure 3. Engine dynamometer arrangement (Exhaust extraction system removed)

For clarity Figure 3 does not show the exhaust gas collector/muffler and extraction system. In terms of fuel supply, any excess fuel not consumed by the engine is recirculated to fuel pump intake thereby allowing the fuel meter to assess the flow rate of fuel actually entering the engine directly.

Design characteristics for the standard engine are provided in Table 1.

Table.1. Standard engine design data

Swept Volume (cm^3)	342
No. of cylinders	2
Bore (mm)	66
Stroke (mm)	50
Trapped compression ratio (r_{cTrap})	7.1:1
Crankcase compression ratio (r_{cc})	1.5:1
Induction control	Single 6 petal reed valve (steel reeds)
Fuel system	Single diaphragm carburettor
Alternative fuel system	Single point inlet injection upstream of the crankcase
Fuel	Gasoline (with 4% SAE40 two-stroke oil added)
Lubrication system	Total loss (Premixed fuel)
Exhaust system	Short stub pipes

One-dimensional Engine Modelling

The fluid dynamics models of the engine were developed using WAVE (version 2021.3), the one-dimensional code developed by Ricardo (2022). The layout of the representative model can be seen in Figure 4.

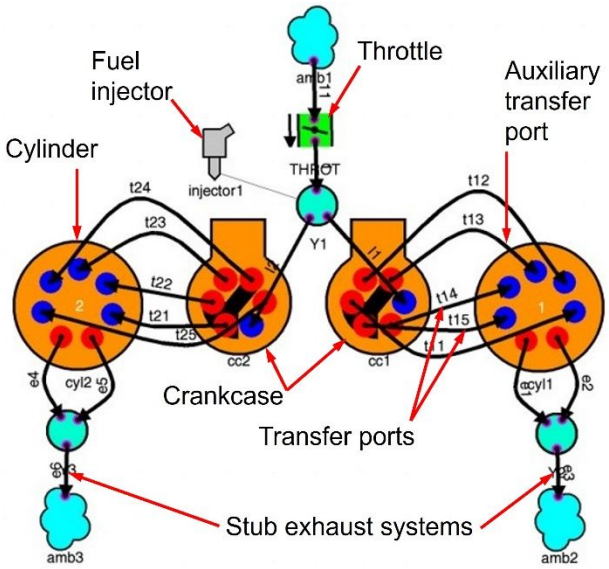

Figure 4. Engine one-dimensional model

The common intake manifold and reed valve block was reflected within the models; however, it was not possible to model the two cylinders from a single crankcase. A model using two crankcases was developed as shown in Figure 4 to circumvent this. The two systems were developed to replicate the compression ratio of the single common crankcase of the real engine. The cylinders use a five-transfer port arrangement that adopts the loop scavenging process developed originally by Schnürle as discussed by Schweitzer (1949) and Hooper (2017a). Each of the ports can be seen to be connected to the crankcases by passages or ducts. Auxiliary transfer port fuel injected models replicated the positioning of the injector at a position 5mm from the cylinder end of the port and therefore close to piston. The injector pulse width was optimised within the model. For inlet injected models a single injector was located feeding into the Y junction between the throttle and crankcase as shown in Figure 4. In response to the computed air mass flow, fuel flow was calculated proportional to a pre-set stoichiometric air:fuel ratio defined within the model. The engine also uses two exhaust ports per cylinder with a central bridge exhausting into short stub pipes of 122 mm length and this arrangement has been recreated in the models.

Model theory

Many two-stroke cycle engines utilise reed valves in order to control the induction charge flow. The engine forming the subject of this study uses a single block six petal reed valve for such purpose feeding the common crankcase. In other words, this single block controls the entire engine air flow or air and fuel for the carburetted or inlet injected engine. The theory behind modelling the reed valve has been previously discussed by Hooper and Al-Shemmeri (2017) building upon the prior research of Morrison *et al* (1971) and Hinds (1978). The reed can be considered as a cantilever of slender cross section. The steel reeds applied in this study were 17.5 mm wide, 25 mm effective length and 0.2 mm thick. Using cantilever beam theory, it is possible to consider the reed motion due to the pressure difference occurring across the valve. Based upon the reed stiffness, the lift and open area at any condition can be calculated. The expression in equation (1), as defined by Morrison *et al* (1971), can be used to determine deflection at the reed tip: -

$$r_{tip} = \frac{\Delta p_r w_r l_r}{8EI} \tag{1}$$

In terms of flow through the reeds, Morrison *et al* (1971) showed that the flow time area can then be calculated from equation (2): -

$$\int A d\theta = \frac{n_r r_{tip} P_w \theta_p}{2} \tag{2}$$

Based upon the work of Hinds (1978), the reed natural frequency can be calculated from equation (3). Values for the $\beta_j l_r$ term in equation (3) relate to the reed modes of vibration with values of 1.875, 4.694, 7.855, 10.996 and 14.137 recommended. Higher than fifth order values can be ignored as discussed by Blair (1996) and Hinds (1978).

$$f_r = \frac{(\beta_j l_r)^2}{2\pi}\sqrt{\frac{EI}{p_r A_b l_r^4}} = \frac{(\beta_j l_r)^2}{2\pi}\sqrt{\frac{Et_r^2}{12 p_r l_r^4}} \tag{3}$$

The reed spring constant, k_r, can be determined from computing equations (3) and (4): -

$$f_r = \sqrt{\frac{k_r}{m_r}} \tag{4}$$

Input of the effective port flow area and reed spring constant, k_r, enables WAVE to simulate the reed block.

The crankcase was modelled as a pump. As previously discussed, two crankcase elements can be seen in Figure 4 whilst only one is employed in the actual engine. Input functions revolve largely around the compression ratio of the crankcase. It was deemed acceptable to continue the model build with two crankcases with the same crankcase compression ratio as that measured from the original engine. The crankcase provides pressurised air to the five transfer ports located in the cylinders. Combustion is spark initiated with spent gas exhausted from the cylinders via two exhaust ports. The flow time-area history of transfer and exhaust ports can be seen in Figure 5.

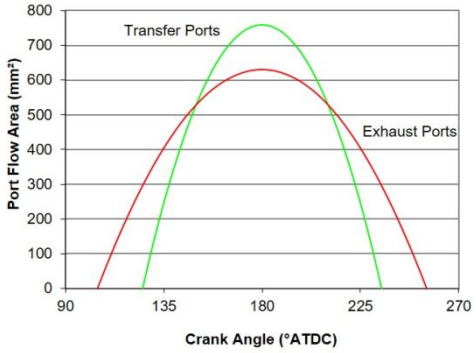

Figure 5. Port flow time - area history

Within a two-stroke cycle engine equipped with ports in the cylinder walls, the flow of air/exhaust is defined by the gas properties and the position of the piston. Port effective flow area can be defined by determining their discharge coefficients (*Cd*) at varying port opening or piston positions. However, Blair (1996) argues that whilst this approach can be used effectively to improve port flow characteristics, it is of limited assistance within one-dimensional fluid dynamic engine models due to limitations of the models to be able to reproduce the actual thermodynamics occurring within the real engine. For this reason, isentropic methods can be adopted.

The port flow area and associated mass flow can be calculated from equations (5) and (6) respectively, as developed by Heywood and Sher (1999): -

$$A_o = w_p h_o - r_p^2\frac{[4-\pi]}{2} \tag{5}$$

$$\dot{m} = \frac{C_d A_r p_o}{\sqrt{RT_o}}\left(\frac{p_R}{p_o}\right)^{\frac{1}{\gamma}}\sqrt{\frac{2\gamma}{\gamma-1}\left(1-\left(\frac{p_R}{p_o}\right)^{\frac{\gamma-1}{\gamma}}\right)} \tag{6}$$

Heywood and Sher (1999) also discuss that for sonic flow, the mass flow is defined by equation (7): -

$$\dot{m} = \frac{C_d A_r p_o}{\sqrt{RT_o}} \sqrt{\gamma} \left(\frac{2}{\gamma + 1} \right)^{\frac{\gamma+1}{2(\gamma-1)}} \tag{7}$$

When computing cylinder flow via transfer ports, the pressure p_R is taken to be the value occurring in the cylinder whilst stagnation pressure, p_o, is set to the scavenge flow pressure. For exhaust flow via the exhaust ports, the stagnation pressure, p_o, is conversely set at the cylinder pressure and p_R, is set to the exhaust pressure. As the port pressure ratio varies the C_d value varies significantly. Heywood and Sher (1999) found that the steady flow C_d value is normally higher than the comparative value determined via unsteady flow conditions. Within WAVE it is possible to define flow coefficients where data is available. A key input function was taken from the engine porting analysis shown in Figure 5 to define flow areas and timing of all modelled ports.

The work of Wiebe (1967) established the formula in equation (8) for assessment of the mass fraction burnt by the combustion process. This formula forms the basis of calculations within WAVE. Ghojel (2010) further discusses the research of Wiebe.

$$x(\theta) = 1 - exp\left[-\left[\frac{c(\theta - \theta_0)}{\Delta\theta_b} \right]^{-b} \right] \tag{8}$$

The research of Heywood and Sher (1999) analysing similar crankcase scavenged spark ignition two-stroke cycle engines has been used to influence the Wiebe function development within this study. Sher (1984) identified values for *b* and *c* of 5 and 3 to 3.2 respectively following combustion rate analysis of the engines in question. In the absence of specific data for the subject engine this prior research has been considered here.

A critical aspect of any engine model is within the assumptions for heat transfer. In the WAVE models the following calculation for heat transfer coefficient, *h*, was used: -

$$h = 0.0128\ D^{-0.2}\ P^{0.8}\ T^{-0.53}\ v_{ch}{}^{0.8} C_m \tag{9}$$

Equation (9) is derived from the research of Woschni (1967). The mean piston speed was found by Woschni to be able to equate to the characteristic gas speed, v_{ch}. The variable C_m, in equation (9) is a scaling factor based upon cylinder bore diameter. If for example the piston crown has a flat non-domed design the value for C_m would be unity, as it was for the subject engine. The combustion chamber is a concentric recess as can be seen in Figure 1. The surface area of the chamber was analysed resulting in a value for C_m of 1.315.

The Colburn analogy as defined by Bird *et al* (2002), and shown in equation (10), is used by WAVE to calculate heat transfer in areas remote from the cylinder.

$$h = \frac{C_f}{2} p U c_p P_r^{-\frac{2}{3}} \tag{10}$$

An allowance for engine friction within WAVE is provided by the expression developed by Chen and Flynn (1965) and shown in equation (11). Unfortunately, Morse test (Stone, 2012) data was unavailable for the engine so values for friction mean effective pressure (p_f) typical for crankcase scavenged engines were used in this study to make the correlation representative here.

$$p_f = c_1 + c_2(p_{max}) + c_3 \frac{Ns}{2} + c_4 \left(\frac{Ns}{2} \right)^2 \tag{11}$$

The WAVE combustion knock sub-model used for the research presented in this Paper is based upon the induction time correlation developed by Douaud and Eyzat (1978). At each timestep within the model the ignition delay or induction time, τ, is calculated via the expression shown in equation (12): -

$$\tau = 0.01869 A_p \left(\frac{O_N}{100}\right)^{3.4017} {p_{cyl}}^{-1.7} \, exp\left(\frac{3800/A_T}{T_{unb}}\right) \tag{12}$$

A key input to equation (12) is the octane number, O_N, of the fuel defined by the user in the WAVE model. A_p is a multiplier defined by the user, p_{cyl} is the cylinder pressure, A_T is a user entered multiplier for activation temperature and T_{unb} is the temperature of the unburned gas fraction in the cylinder. When knock is detected, the user is notified.

As the combustion cycle advances the ignition delay, τ, reduces and the temperature increases in the unburnt mixture. If the flame arrival time is greater than the induction time auto-ignition will occur or when the condition defined by equation (13) is met: -

$$\int_{t_0}^{t_i} \frac{d\tau}{\tau} = 1 \tag{13}$$

The integral limits defined by equation (13) are the auto-ignition (t_i) and end gas compression (t_o) start points. During the simulation the integral is evaluated with time, t_i, being the current instantaneous time of the simulation. Time, t_i, is then ultimately determined when the integral reaches the unity value.

A post detonation burn acceleration can be defined. When this is set, a rate of burn for the spontaneous combustion mass is returned to the cylinder. This causes an increase in temperature and pressure in the cylinder and an increase in heat transfer coefficient within the cylinder. This then defines a post detonation burn time, τ_{post}, defined by equation (14): -

$$\tau_{post} = f_t \left[\frac{0.8573}{B_0(1 + A/F)} exp\left(\frac{T_{act}}{T_{af}}\right)\right] \tag{14}$$

In equation (14); f_t, is a multiplier for the burn scale for post knock occurrence, B_0, is a frequency factor (2233 x 10^3 Hz), A/F, is the air:fuel ratio, T_{act}, is the activation temperature and T_{af}, is the adiabatic flame temperature.

During the post knock phase the rate of fuel burn is calculated from equation (15): -

$$\dot{m}_{fuel} = \frac{m_{vap} + m_{liq}}{\tau_{post}} \tag{15}$$

Similarly the burn rate of the air in the cylinder is calculated from equation (16): -

$$\dot{m}_{air} = \dot{m}_{fuel}(A/F) \tag{16}$$

In equation (15) m_{vap} and m_{liq} are the unburned fuel vapour and unburned liquid fuel masses at the point of knock occurrence. The formulae presented in equations (11) to (16) were developed by Douaud and Eyzat (1978).

The modelling and experimental work presented in this paper builds upon the prior published work of Hooper and Al-Shemmeri (2017c).

Results

Gasoline baseline testing with the standard Mikuni BN-34-30 carburettor was established to 7000 RPM with and without a low resistance exhaust system collector/muffler, fabricated in order to reduce noise levels. This was done to ensure that the collector/muffler system was not affecting the engine's normal operation with the standard 122 mm stub pipes. The results of initial baseline tests are shown in Figure 6. The experimental test

data was recorded using 98RON gasoline with synthetic two-stroke oil added to the fuel in the recommended ratio of 25:1.

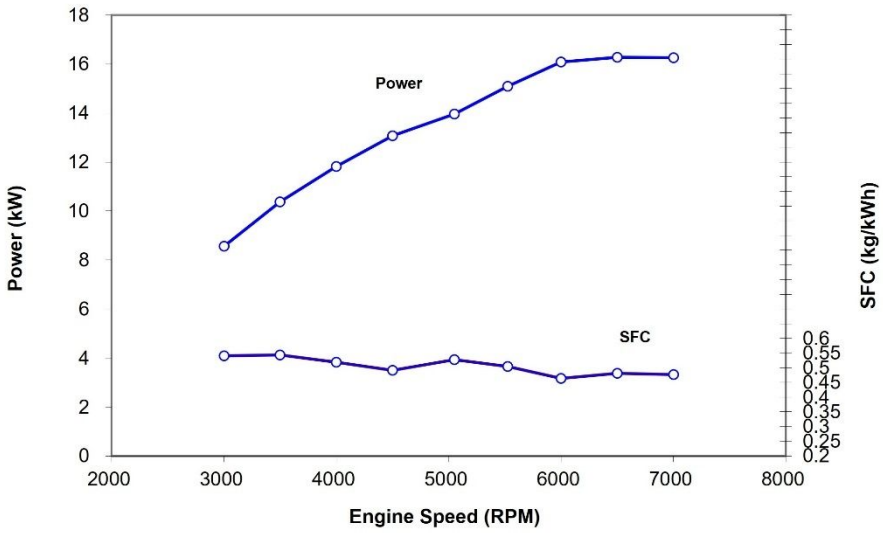

Figure 6. Initial experimental baseline test data of engine recorded using carburettor fuelling with 98RON gasoline with 25:1 oil premix

On reference to Figure 6, the maximum power from the experimental testing can be seen to occur at 6500 RPM with a value of 16.27 kW. The minimum full load SFC occurs at 6000 RPM with a value of 0.464 kg/kWh.

Testing with indirect injection into the auxiliary transfer ports was then performed. Again the fuel used was 98RON gasoline but as this point of fuel introduction bypasses some of the critical components that require the oil for lubrication an alternative means of lubrication was required. A precision metering system was calibrated in order to provide a separate supply of lubricating oil into the intake manifold just upstream of the engine reed valve. This was metered to replace the 4% oil that would otherwise be present in the intake fuel supply. The pump was driven from the dynamometer shaft as shown in Figure 3 to simplify the installation. Oil delivery was fed to the common intake manifold just upstream of the reed valve.

Auxiliary port fuel injection (API)

Injection of fuel via the transfer port area of a two-stroke engine involves a limited time availability for successful unhindered delivery of the fuel charge. Injection has to be synchronised with the port open phase defined by the period of the piston uncovering the port on the down stroke and closing the port on the up stroke. The time window is far less constrained with direct injection (DI) into the combustion chamber, however; DI systems can present a higher mass penalty in terms of the associated hardware required.

Initially relatively low flow rate injectors were used as the metering supply. Unfortunately the delivery at normal operating pressures of 2.75 bar were insufficient. Fuel pressure was increased to 7.25 bar to reduce injector pulse widths. Larger capacity injectors were then installed which were capable of supplying sufficient fuel in the short time available. Figure 7 shows kerosene performance data for the engine using the lower capacity L231 injectors at 7.25 bar, and higher capacity R588 injectors at 2.75 bar.

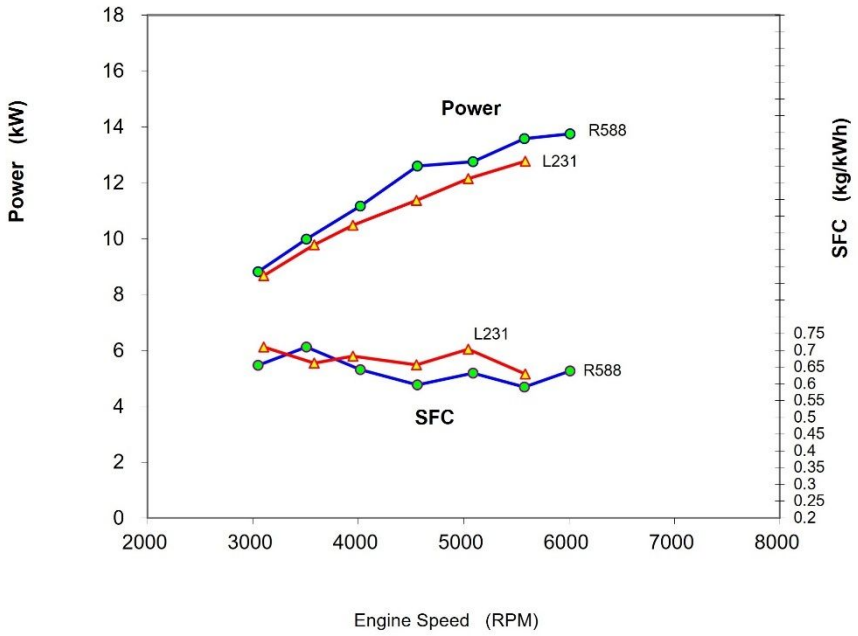

Figure 7. Comparison of experimental kerosene JET A-1 performance using high (R588) and low (L231) flow rate injectors

Initial testing on kerosene was limited to speeds of 6000 RPM due to the onset of combustion knock above 6100 RPM. Using the lower capacity injectors, 5500 RPM was found to be the limiting speed achievable before knock was observed. It should be pointed out that testing below 3000 RPM would usually exhibit increased knock intensity and for this reason the full load engine speed was only explored from 3000 RPM and above. On reference to Figure 7, full load performance at 5000 RPM is 12.14 kW and SFC 0.704 kg/kWh using the L231 injectors, with 12.76 kW and SFC 0.632 kg/kWh using the R588 injectors.

Table 2 shows comparative pulse width and port open time duration for the two injectors.

Table 2. Port Open time and injector pulse width

Engine speed (rpm)	Port Open Time (ms)	L231 injector pulse width (ms)	R588 injector pulse width (ms)
3000	5.50	4.05	3.51
3500	4.71	3.85	3.57
4000	4.13	3.87	3.00
4500	3.67	3.56	2.83
5000	3.30	3.55	2.63
5500	3.00	3.33	2.57
6000	2.75		2.52
6500	2.54		
7000	2.36		

The calculated port open times in Table 2 are determined from the transfer port timing and relevant engine speed. The reduction in port open time with increasing speed can be readily seen. It can also be seen that the injector pulse width with L231 injectors exceeds the port open time above 5000 RPM. Using the R588 injectors with higher flow capacity the reduced corresponding pulse width and hence ability to inject fuel without

impinging on the piston during the port open period is clear to see. This allowed operation up to 6000 RPM and explains the improved SFC observed in Figure 7 with RAM injectors.

One-dimensional modelling of auxiliary port fuel injection

Models of the engine constructed within the architecture of Ricardo WAVE have been configured to examine differing fuel injection methods. A range of models were developed with a pulse width injector located in each auxiliary port.

The model was developed initially to operate on indolene (Zigler *et al* (2011)) fuel, a reference grade form of gasoline. This fuel is a readily available fuel selectable within the WAVE software fuel definition model. It is also possible to generate new fuels, or blends of fuels, using key thermodynamic properties of the fuel. Kerosene JET A-1 was used for all heavy fuel experimental testing and is similar to AVTUR apart from anti-icing inhibitors to allow high altitude military use. After researching relevant data for the properties for the fuel composition (carbon, hydrogen content), lower heating value, density, entropy of formation, specific heat and heat of vaporisation.

Output performance data using inlet injection (II) and auxiliary port fuel injection (API) of indolene is shown in Figure 8. The experimental data recorded with carburetted 98RON gasoline is also shown for comparative purposes.

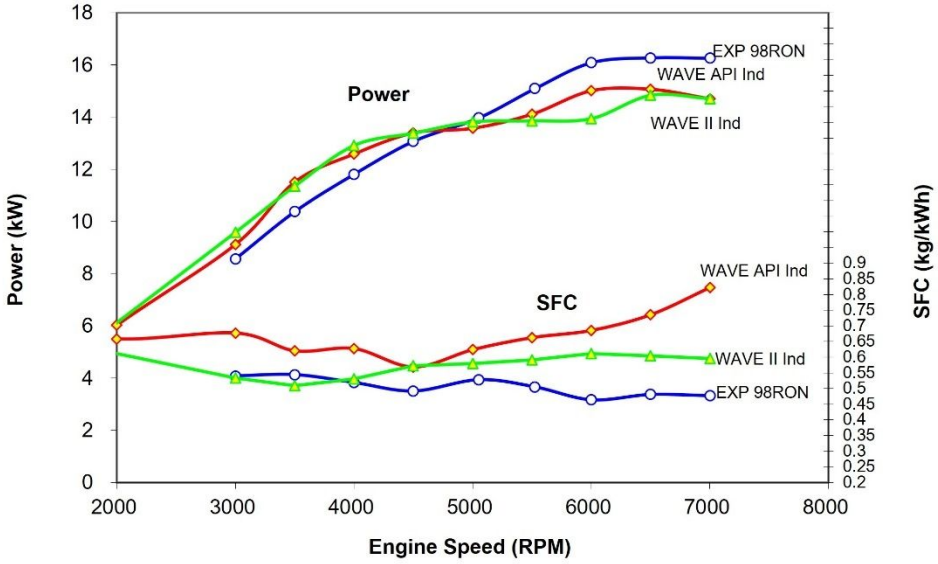

Figure 8. Comparison of 98RON gasoline experimental (EXP) data with WAVE modelled Auxiliary port injection (API) and inlet injection (II) of indolene

It can be seen from Figure 8 that a reasonable correlation between the experimental results and modelled data has been achieved in the medium speed range from 3000 to 5000 RPM although a marked improvement in power with the WAVE model is exhibited at 3500-4000 RPM. Above 5000 RPM the actual data from experimental testing with the diaphragm carburettor demonstrated higher power with a maximum 16.27 kW recorded at 6500 RPM. Using the WAVE models; inlet injected indolene demonstrates a maximum power of 14.84 kW at 6500 RPM whilst auxiliary port injection achieves a higher output of 15.07 kW at 6500 RPM. Specific fuel consumption is lowest with the diaphragm carburettor used in experimental testing with the minimum value being 0.464 kg/kWh occurring at 6000 RPM. A much higher SFC at speeds above 4000 RPM can be seen for inlet injected indolene, although very good correlation can be seen from 3000 – 4000 RPM. On reference to Figure 8 the minimum WAVE modelled SFC with inlet injection can be seen to be 0.508

kg/kWh at 3500 RPM. Using WAVE modelled auxiliary port injection, a significantly higher SFC is evident. The minimum being 0.569 kg/kWh at 4500 RPM.

Predicted cylinder pressure and torque for inlet injection and auxiliary port injection of indolene are presented in Figures 9 and 10 respectively. The data for all cases is at 6000 RPM.

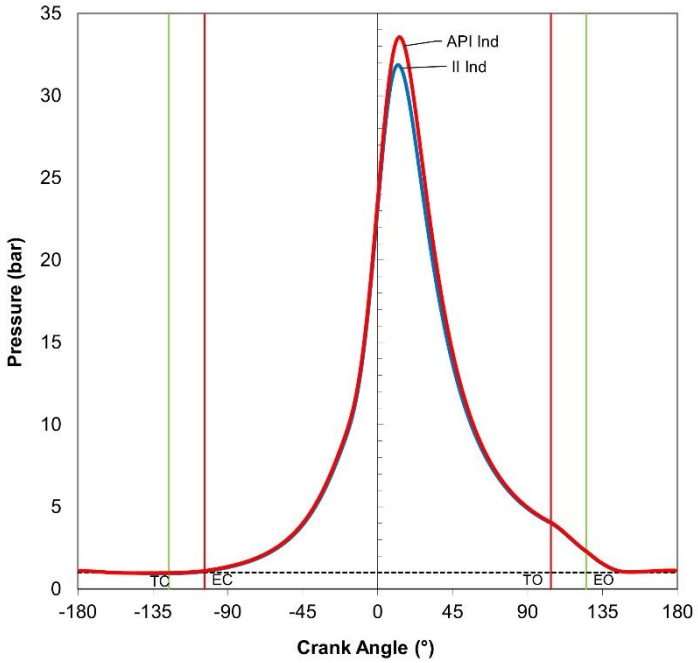

Figure 9. Comparison of cylinder pressures with WAVE modelled Auxiliary port injection (API) and inlet injection (II) of indolene at 6000 RPM

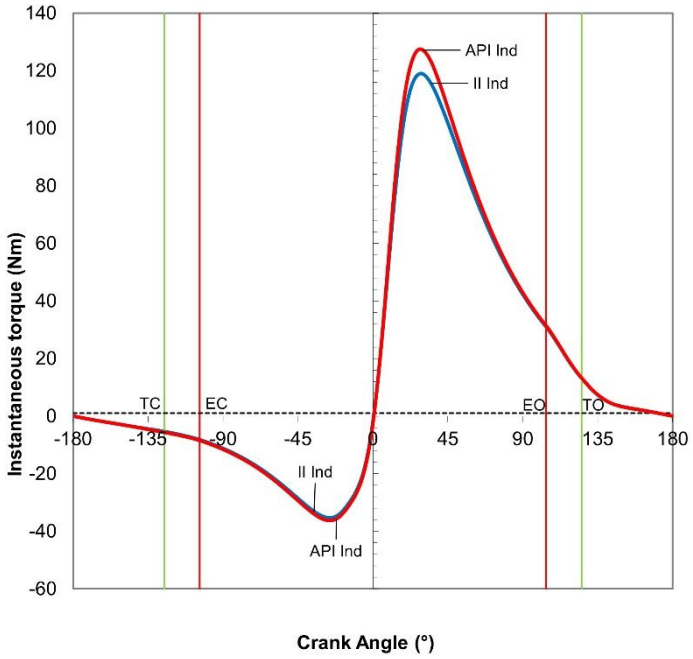

Figure 10. Comparison of instantaneous torque predictions with WAVE modelled Auxiliary port injection (API) and inlet injection (II) of indolene at 6000 RPM

The maximum cylinder pressure, shown in Figure 9, for inlet injection is 31.9 bar occurring at 12.2° ATDC. For the auxiliary port injected model, the maximum cylinder pressure can be seen to have increased to 33.5 bar and occurs at 13.1° ATDC. In terms of the predicted torque throughout the same cycles the peak positive torque is 119.1 Nm for inlet injection with a peak negative of -35.3 Nm. For the higher output observed for API at 6000 RPM the comparable peak values are 127.5 Nm and -36.2 Nm respectively. The positive torque reflects the positive net energy output from the combustion process whilst the negative torque is an indication of the energy input required to perpetuate engine operation during the intake and compression phases of the cycle.

Experimental effects of compression ratio variation

The susceptibility of an internal combustion engine to suffer from combustion knock increases with lower volatility fuels. This has to be eliminated by retarding the ignition timing and/or reducing the compression ratio. For two-cycle engines the most relevant compression ratio is not the full piston stroke ratio, but the trapped compression ratio (r_{cTrap}). The ratio can be calculated from the following expression.

$$r_{cTrap} = \frac{V_{aEC}}{V_c} \tag{17}$$

The engine has a full geometric stroke compression ratio (r_c) of 9.2:1. This equates to a TCR of 6.74:1. From experimental test experience this level was found to be too high for spark ignited kerosene operation. Fortunately, the engine has a detachable cylinder head. This provides simple adjustment of the combustion chamber volume by alteration of the cylinder head gasket/shimming thickness. Alternative shims were machined giving ratios of 6.00:1 (8.02:1) and 5.65:1 (7.28:1). Problems were experienced with the engine head gaskets, so these were later eliminated by use of one-piece copper shim plates.

Table 3. Experimental full geometric and trapped compression ratios

Full geometric compression ratio (r_c)	Trapped compression ratio (r_{cTrap})
9.20:1	6.74:1
8.02:1	6.00:1
7.28:1	5.65:1

Test data is presented in Figure 11, showing the effect of compression ratio adjustment. At 6.00:1 TCR the ignition timing had to be retarded to approximately 50-60% of normal gasoline advance. However further reduction to 5.65:1 enabled advance to normal gasoline ignition timings. At 5000 RPM, the full load performance shown in Figure 11 is 13.56 kW and 0.651 kg/kWh with 6.00:1 TCR and 13.93 kW and 0.610 kg/kWh with 5.65:1 TCR.

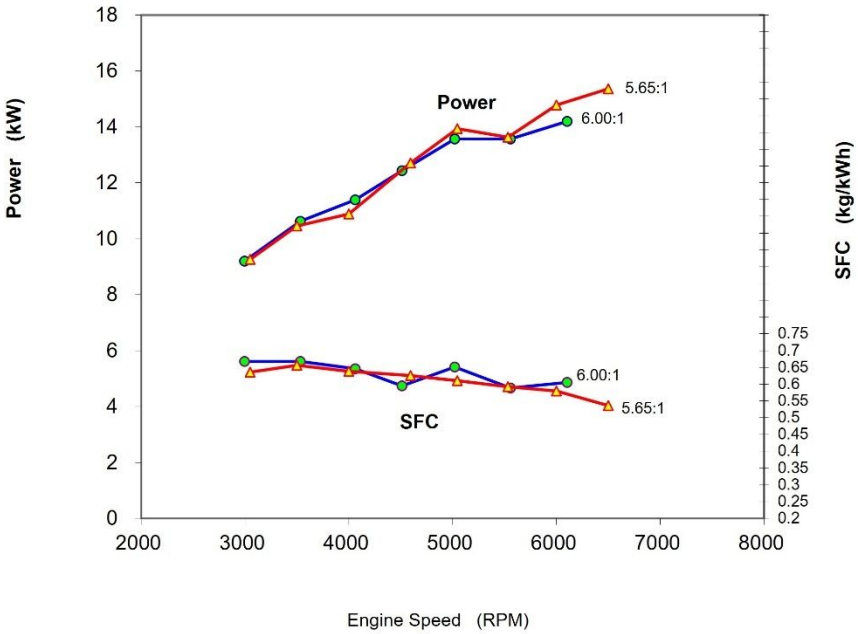

Figure 11. Dynamometer experimental comparison of kerosene JET A-1 injection using 6.00:1 and 5.65:1 trapped compression ratios

One-dimensional modelling of effects of compression ratio variation

Auxiliary port injection of JET A-1

Summarised results of computational modelling of auxiliary port injection (API) of indolene at full compression and JET A-1 at reduced trapped compression ratios of 6.00 and 5.65:1 is compared in Figure 12. Experimental data using carburettor supplied 98RON gasoline is also shown for comparative purposes.

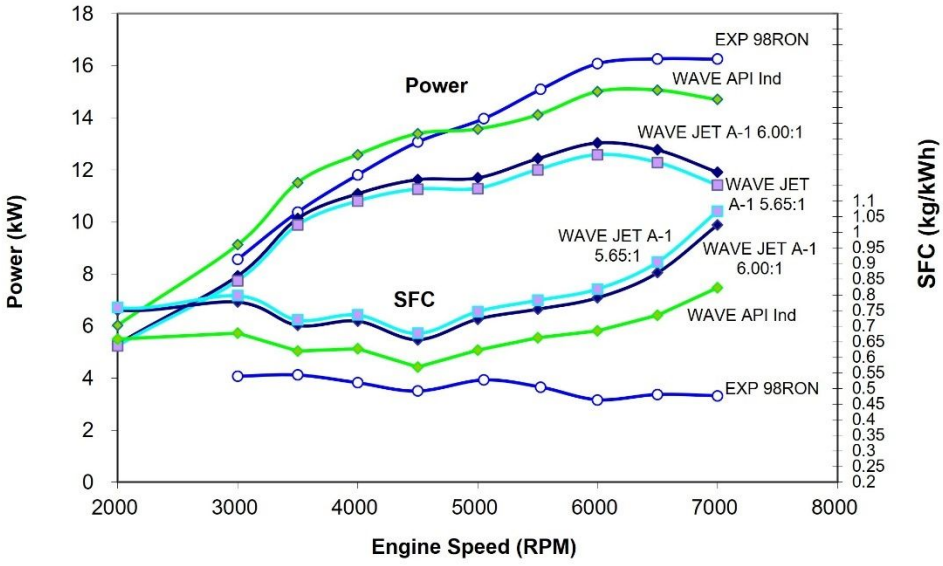

Figure 12. Effect of compression ratio using full compression 98RON gasoline experimental (EXP) data and WAVE modelled Auxiliary port fuel injection of JET A-1 with reduced 6.00:1 (8.02:1) and 5.65:1 (7.28:1) TCR

Simulation data shown in Figure 12 displays the highest maximum power using JET A-1 at 6.00:1 TCR of 13.04 kW at 6000 RPM compared with 12.58 kW at 5.65:1 TCR. The minimum JET A-1 SFC of 0.656 kg/kWh at 4500 RPM is achieved with 6.00:1 TCR compared with 0.677 kg/kWh using 5.65:1 TCR.

WAVE utilises the method of knock prediction derived by Douaud and Eyzat (1978). To determine if knock is occurring WAVE requires values for research octane number (RON) to be input into the activated Douaud and Eyzat sub model. As JET A-1 is not normally used in spark ignition engines no readily available RON values could be located. Contact with Shell Aviation was therefore explored to see if a representative RON value for JET A-1 had ever been determined, however no values had been derived as it is not relevant for the normal use of JET A-1 in turbine engines. However, using correlations derived by Kalghatgi (2005) a potential value for RON of 58.6 has been calculated for a cetane value of 30. This RON value was therefore used in the WAVE models developed using JET A-1 in order to determine if knock was predicted to be occurring. Knock was observed at lower full load engine speeds during the model runs. This could be observed occasionally at 2000 RPM and more so at 1000 RPM in terms of increased knock intensity. For speeds from 3000 RPM and above, no knock was observed.

Figures 13 and 14 present WAVE modelled predictions of cylinder pressure and torque for auxiliary port injection of JET A-1 for the key compression ratios respectively. As for Figures 9 and 10 the data is at 6000 RPM.

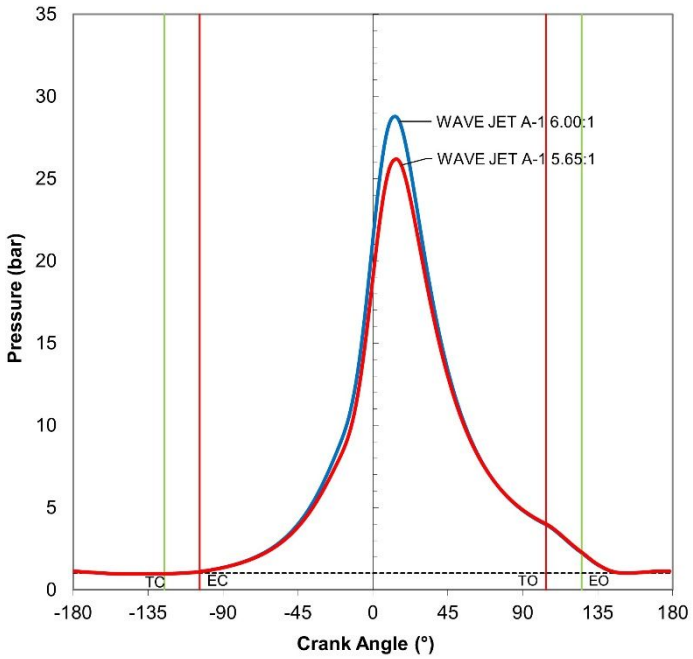

Figure 13. Comparison of cylinder pressures with WAVE modelled Auxiliary port fuel injection of JET A-1 with reduced 6.00:1 (8.02:1) and 5.65:1 (7.28:1) TCR at 6000 RPM

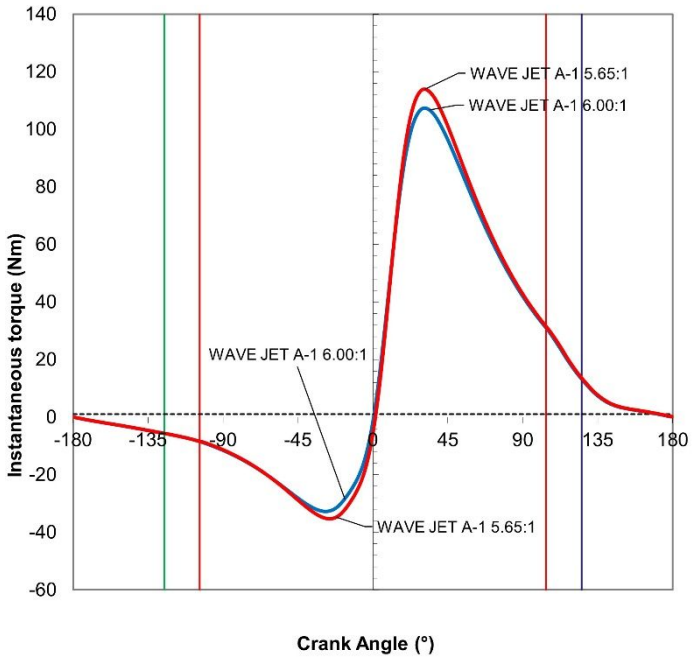

Figure 14. Comparison of instantaneous torque predictions with WAVE modelled Auxiliary port fuel injection of JET A-1 with reduced 6.00:1 (8.02:1) and 5.65:1 (7.28:1) TCR at 6000 RPM

In Figure 13 the maximum cylinder pressure using 6.00:1 TCR is 28.8 bar occurring at 13.1° ATDC. Reducing the TCR to 5.65:1 shows a predicted maximum cylinder pressure of 26.2 bar at 14.1° ATDC. Close examination of the rate of rise of pressure in Figure 13 shows a more rapid increase before TDC and therefore greater compression work for the higher 6.00:1 compression ratio. There is a less pronounced increase in expansion work after TDC. The predicted torque shown in Figure 14 shows a peak positive torque of 107.4 Nm with a TCR of 6.00:1 and a corresponding peak negative of -32.7 Nm. Reducing the TCR to 5.65:1 predicts peak torque values of 113.9 Nm and -35.3 Nm respectively.

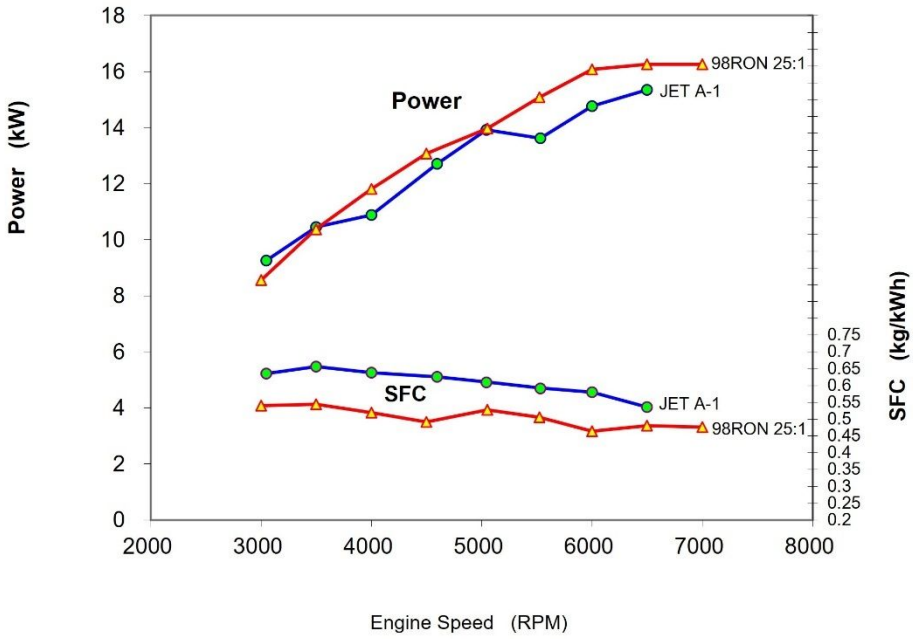

Figure 15. Dynamometer experimental performance comparison of kerosene JET A-1 with carburetted gasoline (98RON 25:1) oil premix fuel

On reference to Figure 15, it can be seen that the experimental recorded power at 5000 RPM is identical with both fuels, however the SFC is increased to 0.593 kg/kWh with kerosene from 0.528 kg/kWh with 25:1 98 RON gasoline/oil mixture. At 7000RPM it was not possible to operate effectively without running into excessive knock using kerosene JET A-1. Testing was therefore limited to a maximum of 6500 RPM.

The density range of the Jet A-1 fuel used for all experimental testing of the subject engine was 792.9 - 799.9 kg/m^3 (measured at 15°C).

All experimental test data recorded from the test engine has been corrected for International Standard Atmospheric conditions (SAE, 2011).

Discussion

The research presented in this paper has considered the application of a simple low mass fuel injection system to a conventional UAV engine. This was done to explore the possibilities of achieving an acceptable outcome meeting the single fuel objectives for military engine powered systems. The effects of introduction of JET A-1 into the cylinder during the open cycle phase around bottom dead centre has achieved some promising results, following compression ratio reduction to avoid combustion knock occurrence and permit advancement of ignition timing to counter what would otherwise be significant performance degradation from the gasoline baseline test data. WAVE modelling exhibited higher occurrence of knock at speeds below 3000 RPM as indeed did the experimental engine on the dynamometer. However due to propeller power plant matching, the engine would not be able to operate at such low speeds at full load in a UAV installation. In practical terms such knock limitations could therefore be avoided.

Baseline testing of the standard gasoline engine with carburettor fuelling established the benchmark for computational modelling of the original engine and dynamometer experimentation with JET A-1 fuelling. The standard gasoline results indicated maximum power of 16.27 kW at 6500 RPM. The inlet injected model correlated closely at 4500-5000 RPM but displayed higher power levels below 4500 RPM. Above 5000 RPM the predicted power output from the model was significantly lower than the actual power output from the test engine of the order of 8.2 to 13.3%, the greatest deviation occurring at 6000 RPM. In terms of SFC, correlation was close below 4500 RPM but deviates from 4500 RPM and above.

Using auxiliary port injection of indolene the results showed a closer correlation at higher speeds in terms of power but less so in terms of SFC. WAVE modelling of auxiliary port injected JET A-1 showed corresponding maximum power predictions of 13.04 kW and 12.58 kW at 6000 RPM using 6.00:1 and 5.65:1 TCR respectively. The modelled SFC using API indicated minimum values of 0.656 kg/kWh and 0.677 kg/kWh at 4500 RPM for 6.00:1 and 5.65:1 TCR respectively. Further work could be conducted to provide a closer correlation of engine friction mean effective pressure within the engine models. Future work to secure data via Morse tests could be incorporated in the WAVE models. This was not possible within the current study. All modelling was therefore conducted with typical values associated with crankcase scavenged two-stroke cycle engines. Dynamometer test data, using JET A-1 delivery via auxiliary port injection, led to a maximum power of 14.19 kW using 6.00:1 TCR. This was observed at a maximum test speed of 6100 RPM with a corresponding SFC of 0.605 kg/kWh. Test speeds above 6100 RPM were not possible due to instability and detonation onset. Reducing the TCR to 5.65:1 allowed operation of the engine at full ignition advance levels typically associated with those achieved with gasoline fuel operation. This allowed a maximum power of 15.35 kW at 6500 RPM with a corresponding SFC of 0.536 kg/kWh to be recorded compared with 16.27 kW and 0.481 kg/kWh at the same speed using gasoline. By reducing the compression ratio a small power increase has been observed at lower engine speeds of 3000 RPM and 3500 RPM when operating on kerosene JET A-1, however at the design maximum power speed, a power loss of the order of 5.7% was apparent.

In terms of thermal efficiency, gasoline offers higher levels due to an ability to operate at lower SFC than has so far been possible operating the engine on kerosene JET A-1. At maximum power the increase in SFC was of the order of 11.4%. The orientation of the engine exhaust ports, directly opposite the auxiliary transfer port, is not ideal for maximising thermal efficiency. For all API models and dynamometer engine tests fuel was introduced as the port opens into the cylinder. The possibility for fuel short-circuiting directly to the exhaust port is a strong possibility with this arrangement and can therefore lead to high specific fuel consumption if the incoming air charge or exiting exhaust gases carries the fuel into the exhaust. Similarly the momentum of the delivered fuel particles can also potentially carry them into the exhaust without any contribution to the

combustion process. Notwithstanding these possibilities, it should also be noted that for the same operating conditions in terms of power and fuel volumetric flow, the specific fuel consumption using kerosene would be higher than that for gasoline due to the higher relative density of kerosene fuel. For this reason alone, operation on kerosene will suffer a 6.6% increase by virtue of its increased density compared with gasoline if volumetric flow rates remain identical.

Applying fuel injection to a crankcase scavenged two-stroke cycle engine, such as the engine used here, requires a fundamental change to the lubrication system. The subject engine used has been previously fuel injected via the inlet tract when applied to the BAE Systems Phoenix UAV system. This method of fuelling can retain the oil-in-fuel lubrication method, however; if the fuel is to be supplied further downstream within the engine, either via the transfer ports as in this study or via direct injection into the combustion chamber, then a separate precision metering pump and lubricant reservoir is required. The overall power plant mass increase with the additional fuel injection hardware therefore also has to allow for the addition of the separate lubrication system and reservoir to provide sufficient lubricant for the duration of a long endurance mission.

It should be pointed out that this type of lubrication system, commonly developed for two-stroke engine motorcycles, has to be applied to Wankel rotary combustion engines, however they are fuelled. It is therefore not a major disadvantage when compared with competing UAV engine types but it does erode some of the simplicity and minimal power plant system volume that a two-stroke cycle engine offers. There are alternatives to this addition to the crankcase scavenged engine whilst retaining the inherent advantages of a two-stroke operating cycle. If the scavenging system is segregated as demonstrated by the prior research of Hooper *et al* (2011) and Stone (2012). This type of engine utilises twin diameter or stepped pistons enabling complete separation of the crankcase and hence the lubrication system. These engines never have to operate with oil in the fuel and allow an isolated lubrication system to be located within the lower section of the engine as is common practice in four-stroke cycle engines.

Computational modelling of the experimental engine within the environment of Ricardo WAVE has provided interesting support and further exploration of the experimental test experience. WAVE is extensively used for the simulation of poppet valve four-stroke engines but is not well known for simulation of crankcase scavenged two-stroke engines and various adaptations have been required in order to successfully simulate the engine within the one-dimensional code.

Conclusions

Fluid dynamic modelling of a twin cylinder 342 cm^3 crankcase scavenged two-stroke cycle engine in support of dynamometer experimental testing using gasoline and JET A-1 kerosene fuels has been conducted to explore validation of the computational models with particular focus on the effects of trapped compression ratio. Whilst it was possible to operate the test engine on JET A-1 at lower speeds without physical adjustment to the TCR this was only possible after significantly retarding the ignition timing to avoid the onset of detonation. The retardation therefore severely reduced engine performance from the baseline gasoline results. Reducing the TCR enabled full ignition advance to be re-applied without the engine suffering from detonation problems. Following optimisation of the trapped compression ratio, the maximum power recorded using JET A-1 from the experimental engine was 15.35 kW at 6500 RPM with a corresponding specific fuel consumption of 0.536 kg/kWh equating to a power loss of 5.7% and an increase in SFC of 11.4% from standard gasoline performance levels. Corresponding maximum power from the same TCR models was 12.58 kW at 6000 RPM. Computational modelling demonstrated reasonable correlation particularly a lower engine speeds but less so at high speeds. The models are considered a good basis for future development to further improve their correlation with additional future experimental experience. Delivery of JET A-1 via the auxiliary transfer ports offers a lower cost alternative to direct injection methods, however the possibility for fuel short-circuiting is greater with this methodology than for direct in-cylinder injection approaches. Greater thermal efficiency is therefore possible with direct injection which has to be considered together when the overall fuel system mass increase is assessed. Direct injection normally requires higher fuel pressures which by necessity increases the mass of fuel pumps, injectors and associated hardware.

Acknowledgements

The support provided by Ricardo for the provision of WAVE is gratefully acknowledged by the author enabling the simulations performed during the study reported in this paper.

References

Austin, R (2010) – “Aircraft Systems – UAS Design, Development and Deployment” (Wiley International ISBN 978-0-470-05819-0 (2010))

Blank, D.A., Pouring, A.A., and Lu, J. (2001) - “Qualitative Flow Field Studies of Combustion in I.C. Engines Using a Simplified Sonex Bowl-in-Piston Geometry” (SAE Paper No. 2001-26-0021 (2001))

Bird, R.B., Stewart, W.E. and Lightfoot, E.N. (2002) - "Transport Phenomena" (2nd edition, Wiley, 2002)

Blair, G.P. (1996) - "Design and Simulation of Two-stroke Engines", (SAE International, Warrendale, Pennsylvania, 1996).

Blundell, D., Turner, J., Pearson, R., Patel, R. and Young, J. (2010) – “The Omnivore Wide-range Auto-Ignition Engine: Results to Date using 98RON Unleaded Gasoline and E85 Fuels” SAE Paper No. 2010-01-0846 (2010)

Chen, S. K. and Flynn, P. (1965) – “Development of a Compression Ignition Research Engine” (SAE Paper No. 650733, 1965)

Davis, E.E. (1991a) – “Combat Tested/Combat Proven Unmanned Aerial Vehicles” (9th International RPV Conference, Bristol, 9-11 September 1991)

Douaud, A. M. and P. Eyzat. (1978) – "Four-Octane-Number Method for Predicting the Anti-Knock Behaviour of Fuels and Engines" (SAE Paper 780080 (1978))

Duddy, B., Lee, J., Walluk, M., and Hallbach, D. (2011) - "Conversion of a Spark-Ignited Aircraft Engine to JP-8 Heavy Fuel for Use in Unmanned Aerial Vehicles," SAE Int. J. Engines 4(1):82-93, 2011, https://doi.org/10.4271/2011-01-0145.

Duret, P., Ecomard, A., and Audinet, M. (1988) – “A New Two-Stroke Engine with Compressed_Air Assisted Fuel Injection for High Efficiency Low Emissions Applications” SAE Paper No.880176 (SAE International Congress and Exposition, Detroit, Michigan Feb 1988)

Ghojel, J.I. (2010) - "Review of the development and applications of the Wiebe function: a tribute to the contribution of Ivan Wiebe to engine research" (IMechE International Journal of Engine Research Vol. 11, Issue 4, 2010) DOI: 10.1243/14680874JER06510

Goraj, Z. and Frydrychewicz, A. (2004) - ‘‘Development Approach of the PW-103. An Increased Reliability Male UAV Under the CAPECON Project within the V FR of EU" (Proceedings of the 24th International Conference of Aeronautical Sciences, Yokohama, Japan, 29 August - 3 September 2004)

Heywood, J.B. & Sher, E. (1999) – “The Two-Stroke Cycle Engine: It’s Development, Operation and Design” (Taylor and Francis / SAE International ISBN 0-7680-0323-7 (1999))

Hinds, E.T. (1978) - “Intake Flow Characteristics of a Two-Stroke Cycle Engine fitted with Reed Valves” (PhD Thesis, Queen’s University of Belfast, August 1978)

Hooper, B. and Favill, J.E. (1978) - “Modern stepped piston engines” (IMechE Paper No.C133/78 Design and Development of Small IC Engines Conference, 31 May - 2 June 1978)

Hooper, P.R. (2019) - “Low Noise, Vibration and Harshness Solutions for in-Line Three-Cylinder Range Extender and Hybrid Electric Vehicles.” (International Journal of Engine Research 2019). https://doi.org/10.1177/1468087419859084

Hooper, P. (2017a) - "Low Volatility Fuel Cold Start Experience with a Stepped Piston UAV Engine to Address Single Fuel Objectives," (SAE International Journal of Engines 10(4):2017. SAE Technical paper 2017-01-9283, DOI: 10.4271/2017-01-9283) <http://papers.sae.org/2017-01-9283/>

Hooper, P.R. (2017b) - "Experimental experience of cold starting a spark ignition UAV engine using low volatility fuel", (Aircraft Engineering and Aerospace Technology, Vol. 89 Iss: 1, pp.106 – 111)

DOI http://dx.doi.org/10.1108/AEAT-09-2014-0137

Hooper, P.R., and Al-Shemmeri, T. (2017c) - "Improved efficiency of an unmanned air vehicle IC engine using computational modelling and experimental verification", (Aircraft Engineering and Aerospace Technology, Vol. 89 Iss: 1, pp.184 – 192) DOI http://dx.doi.org/10.1108/AEAT-09-2015-0200

Hooper, P.R., Al-Shemmeri, T., and Goodwin, M.J. (2011) – "Advanced modern low emission two-stroke cycle engines" (Proceedings of the Institution of Mechanical Engineers, Part D: Journal of Automobile Engineering. Vol. 225 No.11, November 2011)

Hooper, P.R., Al-Shemmeri, T., and Goodwin, M.J. (2012) – "An experimental and analytical investigation of a multi-fuel stepped piston engine" (Journal of Applied Thermal Engineering April 2012) <http://dx.doi.org/10.1016/j.applthermaleng.2012.04.034>

Kalghatgi, G.T. (2005) – "Auto-ignition quality of practical fuels and implications for fuel requirements of future SI and HCCI engines" (SAE Paper No. 2005-01-0239 (2005))

Kalkstein, J., Röver, W., Campbell, B., Zhong, L., Huang, H., Ping Liu, J., Tatur, M., Geistert, A., and Tusinean, A. (2006) - "Opposed Piston Opposed Cylinder (opoc™) 5/10 kW Heavy Fuel Engine for UAVs and APUs" (SAE Paper No. 2006-01-0278 SAE 2006 World Congress & Exhibition, Detroit April 2006)

Kucinski, W. (2018) - "So you want to Design Engines: UAV Propulsion Systems" (SAE International ISBN: 978-0-7680-9175-5)

Kweon, C. B. M. (2011) - "A Review of Heavy-Fueled Rotary Engine Combustion Technologies" (No. ARL-TR-5546. Army Research Laboratory Aberdeen Proving Ground MD.) < https://apps.dtic.mil/dtic/tr/fulltext/u2/a545309.pdf >

Liu, R., Wei, M., and Yang, H. (2016) - "Cold start control strategy for a two-stroke spark ignition diesel-fuelled engine with air-assisted direct injection" (Applied Thermal Engineering 108 (2016) pp414-426)

Liu, R., Wei, M., Wang, C., and Huang, T. (2019) - "Fuel Flow Control for Starting a Crankcase-Injected Two-Stroke Spark Ignition Engine Fueled with Kerosene (RP-3)" (Journal of Energy Engineering/Volume 145 Issue 4 - August 2019)

Malriat, J., Hill, W., Soimar, M and Christ, A. (1991b) – "Heavy Fuel Development for the Joint Unmanned Aerial Vehicle Program" (9th International RPV Conference, Bristol, 9-11 September 1991)

Mattarelli, E., Rinaldini, C., and Baldini, P. (2014) - "Modeling and Experimental Investigation of a 2-Stroke GDI Engine for Range Extender Applications," (SAE Technical Paper 2014-01-1672, (2014), doi:10.4271/2014-01-1672.)

McDonald, C.F., Massardo, A.F., Colin Rodgers, C., and Stone, A. (2008) - "Recuperated gas turbine aeroengines. Part III: engine concepts for reduced emissions, lower fuel consumption, and noise abatement" (Aircraft Engineering and Aerospace Technology, Vol. 80 No. 4, pp. 408-426) DOI: https://doi.org/10.1108/00022660810882773

Morrison, J.L.M. and Crossland, B. (1971) – "An Introduction to the Mechanics of Machines" (2nd Edition Longman, ISBN 978 0582447295 (1971))

Owens, E., LePera, M., and Lestz, S. (1989) - "Use of Aviation Turbine Fuel JP-8 as the Single Fuel on the Battlefield," SAE Technical Paper 892071, 1989, doi:10.4271/892071

Ricardo PLC website (2022) – WAVE simulation software information available from:- <https://software.ricardo.com/products/wave/wave-engine-performance> [accessed 14 April 2022]

SAE (2011) - "J1349 Engine power test code – spark ignition and compression ignition – net power rating" (Warrendale, Pennsylvania: SAE International, 2011)

Schlunke, K.(1989) – "The Orbital Combustion Process Engine" (10th Vienna Motorsymposium, VDI No. 122, pp63-68, 1989)

Schweitzer, P.H. (1949) – "Scavenging of Two-Stroke Diesel Engines" (The Macmillan Company, New York (1949))

Sher, E.(1984) – "The Effect of Atmospheric Conditions on the Performance of an Airborne Two-Stroke Spark Ignition Engine" (Proc. Inst. Mech. Eng., Part D, Vol 198, No. 15 pp 239-251, 1984)

Stone, R. (2012) - Introduction to Internal Combustion Engines, 4th Edition (Palgrave MacMillan) ISBN: 9781137028297 (2012)

Turan, O. (2012) - "Exergetic effects of some design parameters on the small turbojet engine for unmanned air vehicle applications" (Energy, The International Journal, 46 (2012), pp. 51-61)

Turner, J., Blundell, D., Pearson, R., Patel, R. Larkman, D., Burke P., Richardson, S., Green, N.M., Brewster, S., Kenny, R. and Kee, R. (2010) – "Project Omnivore: A Variable Compression Ratio ATAC 2-Stroke Engine for Ultra-Wide-Range HCCI Operation on a Variety of Fuels" SAE Paper No. 2010-01-1249 (2010)

US Department of Defense Directive 4130.43 (1988) - "Fuel Standardization," Office of the Secretary of Defense, Washington, DC, 1988.

Wiebe, I. (1967) – "Halbempirische Formel für die Verbrennungsgeschwindigkeit" (Verlag der Akademie der Wissenschaften der UdSSR, Moscow, 1967)

Work, F (2011) - "Development of multi-fuel, power dense engines for maritime combat craft" (Journal of Marine Engineering & Technology, Vol 10 Issue 2, 37-46)

Woschni, G. (1967) – "A universally applicable equation for the instantaneous heat transfer coefficient in the Internal Combustion Engine" SAE Paper No.670931 (SAE Transactions., Vol 76, pp 3065, 1967)

Xu, Z., Ji, F., Ding, S., Zhao, Y., Zhou, Y., Zhang, Q., and Du, F. (2021) - "Digital twin-driven optimization of gas exchange system of 2-stroke heavy fuel aircraft engine" (Journal of Manufacturing Systems, Volume 58, Part B, January 2021, pp132-145) <https://doi.org/10.1016/j.jmsy.2020.08.002>

Zigler, B. T., Keros, P. E., Helleberg, K. B., Fatouraie, M., Assanis, D., and Wooldridge, M. S. (2011) - "An experimental investigation of the sensitivity of the ignition and combustion properties of a single-cylinder research engine to spark-assisted HCCI" (International Journal of Engine Research, 12(4), 353-375)

Nomenclature

Symbols

A	Cross sectional area
A_b	Reed bending plane cross sectional area
A/F	Air:fuel ratio
A_o	Open port area
A_p	Knock multiplier
A_r	Geometric open port area
A_T	Activation temperature multiplier
b	Constant
B_0	Frequency factor
c	Constant
$c_{1,2,3,4}$	Constants
C_d	Discharge coefficient
C_d	Flow coefficient

C_m	Relative heat transfer area scaling factor
c_p	Constant pressure specific heat
D	Cylinder diameter
D_R	Delivery ratio
E	Modulus of Elasticity
f_r	Reed natural frequency
f_t,	Burn scale post knock multiplier
h	Heat transfer coefficient
h_o	Port open height
I	Second moment of area
k_r	Reed spring constant
l_r	Reed length
$\dot{m}$	Mass flow rate
m_r	Reed mass (lift portion)
m_{liq}	Unburned liquid fuel mass
m_{vap}	Unburned fuel vapour mass
N	Engine speed
n_r	Number of reeds
O_N	Fuel research octane number
p_{cyl}	Cylinder pressure
p_f	Friction mean effective pressure
p_{max}	Maximum cylinder pressure
p_o	Upstream stagnation pressure
p_f	Friction mean effective pressure
p_{max}	Maximum cylinder pressure
p_r	Gas pressure at reference condition
p_R	Pressure at restriction
P	Instantaneous gas pressure
P_r	Prandtl number
P_w	Reed port width
r_c	Compression ratio
r_{cc}	Crankcase Compression Ratio
r_{cTrap}	Trapped compression ratio
R	Universal gas constant
r_p	Port corner radius
r_{tip}	Deflection at reed tip
s	Stroke
t_i	Start time of auto-ignition
t_o	Start time of end gas compression
t_r	Reed thickness
T	Instantaneous gas temperature
T_{act}	Activation temperature
T_{af}	Adiabatic flame temperature
T_o	Upstream stagnation temperature
T_{unb}	Temperature of the cylinder unburned gas fraction
w_p	Width of port
w_r	Reed petal width normal to flow
V_c	Clearance volume
V_{aEC}	Swept volume after exhaust port closure
v_{ch}	Characteristic gas velocity
$x(\theta)$	Mass fraction burned at crank angle θ
$\beta_j l_r$	Reed vibration mode
$\Delta\theta_b$	Duration of combustion
θ	Crank angle θ_0 Crank angle at start of combustion
θ_p	Reed open period
γ	Ratio of specific heats
τ	Ignition delay
τ_{post}	Post detonation burn time

Definitions, Acronyms and Abbreviations

API	Auxiliary Port Injection
AVTUR	AViation TURbine fuel
BDC	Bottom Dead Centre
BMEP	Brake Mean Effective Pressure
CCR	Crankcase Compression Ratio
DF-2	Diesel Fuel 2
DoD	United States Department of Defense
DI	Direct Injection
EXP	Dynamometer Experimental data
FMEP	Friction Mean Effective Pressure
HFE	Heavy Fuel Engine
II	Inlet Injection
JET A-1	Commercial aviation grade kerosene fuel
JP-5	Jet Propulsion 5 fuel
JP-8	Jet Propulsion 8 fuel
NATO	North Atlantic Treaty Organisation
RON	Research Octane Number
RPM	Revolutions per minute
SFC	Specific Fuel Consumption
SI	Spark Ignition
TCR	Trapped Compression Ratio
TDC	Top Dead Centre
UAV	Unmanned Air/Aerial Vehicle
UAS	Unmanned Air/Aerial System

REVIEWER RESPONSES FROM AEAT

Editor Evaluation: DEADLINE: 26-Jul-2022

Reviewer(s)' Comments to Author:

Reviewer: 1

Recommendation: Major Revision

Comments:

I have examined this new version of paper and I have noticed a significant improvement in the paper presentation and some of the major critics are answered. However, still many of previous queries are unsatisfied. The authors should provide reasonable answers to validate the presented results and improve the quality of this paper to the standard of this quality journal

Queries

The title should be shortened to

Study of the effects of compression ratio on the heavy fuel operated spark ignition engine of an unmanned aerial vehicle

Still there are many linguistic problems; check with an editing service

Still are some grammatical errors; check the present and the past tense use.

Correct in :Design/methodology/approach – One-dimensional fluid dynamic modelling of

Correct in :heavy fuel operation was is equal to15.35 kW at 6500 RPM compared to 16.27 kW

Revise the whole not good: Practical implications – This studied engine forming the basis of this experimental and fluid dynamic simulation is a power plant specifically designed for UAV applications. The validation of the computational model is supported by experimental tests experience gives an ability to explore modifications in terms effects of compression ratio optimisation and heavy fuel injection technology for potential on the solution andlost cost heavy fuel engine and the solutions is supported by experimental tests.

Change here : ..... logistical challenges of the single fuel policy for UAVs.

Change title here : Computational Engine Modelling to 1-D Engine Modelling

Make sure that all the presented equations are correct and add for all of them their origin references, unless are developed by authors and in this case you must say that clearly.

Change here: Unfortunately, Morse (check here you mean more) test data.

Check eqt (13) some thing is missing (illogical)

All figures have large empty spaces due to bad scale range.

Explain why there negative torque value for the readers comprehension.

If there is a real experimental work in this paper you must say that clearly, and provide clear photos of test bench with engine, measurement procedure pickups, and measurements recordings and so on….

Improve your discussion based on in-depth physical analyses, not only describing obtained values and their changes.

Additional Questions:

1. Originality: Does the paper contain new and significant information adequate to justify publication?: Applied of known ideas to a real case

2. Relationship to Literature: Does the paper demonstrate an adequate understanding of the relevant literature in the field and cite an appropriate range of literature sources? Is any significant work ignored?: yes

3. Methodology: Is the paper's argument built on an appropriate base of theory, concepts, or other ideas? Has the research or equivalent intellectual work on which the paper is based been well designed? Are the methods employed appropriate?: yes

4. Results: Are results presented clearly and analysed appropriately? Do the conclusions adequately tie together the other elements of the paper?: The authors should provide reasonable answers to validate the presented results and improve the quality of this paper to the standard of this quality journal

conclusion should be improved

5. Implications for research, practice and/or society: Does the paper identify clearly any implications for research, practice and/or society? Does the paper bridge the gap between theory and practice? How can the research be used in practice (economic and commercial impact), in teaching, to influence public policy, in research (contributing to the body of knowledge)? What is the impact upon society (influencing public attitudes, affecting quality

of life)? Are these implications consistent with the findings and conclusions of the paper?: yes

6. Quality of Communication: Does the paper clearly express its case, measured against the technical language of the field and the expected knowledge of the journal's readership? Has attention been paid to the clarity of expression and readability, such as sentence structure, jargon use, acronyms, etc.: yes

Response to points raised by Reviewers

Manuscript ID AEAT-07-2021-0220

"Study of the effects of trapped compression ratio on the heavy fuel operation of a spark ignition Unmanned Aerial Vehicle engine"

Reviewer's Comments to Author:	Author's response:
Reviewer: 1	*Please note all text modifications have been added as red text.*
The title should be shortened to Study of the effects of compression ratio on the heavy fuel operated spark ignition engine of an unmanned aerial vehicle	Thank you for your comments. The title has been modified.
Still there are many linguistic problems; check with an editing service Still are some grammatical errors; check the present and the past tense use.	Thank you for your comments. I have discussed the past/present tense question with the Journal Editor. Past tense is agreed to be appropriate. I have however made some changes to the text.
Correct in :Design/methodology/approach – One-dimensional fluid dynamic modelling of	The text has been modified to reflect your request.
Correct in :heavy fuel operation was is equal to15.35 kW at 6500 RPM compared to 16.27 kW	The text has been modified to reflect your request.
Revise the whole not good: Practical implications – This studied engine forming the basis of this experimental and fluid dynamic simulation is a power plant specifically designed for UAV applications. The validation of the computational model is supported by experimental tests experience gives an ability to explore modifications in terms effects of compression ratio optimisation and heavy fuel injection technology for potential on the solution andlost cost heavy fuel engine and the solutions is supported by experimental tests.	I have modified the text to accommodate your request.

Change here : ..... logistical challenges of the single fuel policy for UAVs.	Please forgive me but your proposed text appears to be the same as my existing text. I am happy to change to your recommendation if you have a particular requirement.
Change title here : Computational Engine Modelling to 1-D Engine Modelling	Thank you for your comments. The title has been modified.
Make sure that all the presented equations are correct and add for all of them their origin references, unless are developed by authors and in this case you must say that clearly.	References to each formula or set of formulae have been added or clarified.
Change here: Unfortunately, Morse (check here you mean more) test data.	This is actually not a typographical error. The word is Morse. The Morse test is a method for dynamometer assessment of FMEP. I have added a reference to help with clarification.
Check eqt (13) some thing is missing (illogical)	Since receiving your comment I have actually consulted with Ricardo regarding this query. They have confirmed that WAVE uses the same form of equation (13) developed by Douaud and Eyzat. I have added further text to expand the explanation in the Paper which I hope addresses your comment.
All figures have large empty spaces due to bad scale range.	The scales were adjusted to the earlier settings due to another Reviewer's request. I have adjusted the scales further to hopefully try to satisfy both requirements.
Explain why there negative torque value for the readers comprehension.	Explanatory text has been added beneath Figure 10.
If there is a real experimental work in this paper you must say that clearly, and provide clear photos of test bench with engine, measurement procedure pickups, and measurements recordings and so on….	Text has been added together with an image and schematic of the dynamometer test setup (please see new Figures 2 and 3).
Improve your discussion based on in-depth physical analyses, not only describing obtained values and their changes.	Thank you for you comments. The discussion has been altered in response to your request.
conclusion should be improved	The text of the Conclusions has been revised.